NAVAL POSTGRADUATE SCHOOL
Monterey , California

AD-A232 466

DTIC
S ELECTE
MAR 12 1991
B **D**

THESIS

A STUDY OF PC-BASED HF IONOSPHERIC
PROPAGATION PREDICTIONS FOR USE IN
NAVAL COMMUNICATIONS

by

Georgios H. Giakoumakis

June 1990

Thesis Advisor   Richard W. Adler

91 3 06 038

REPORT DOCUMENTATION PAGE

1a Report Security Classification Unclassified		1b Restrictive Markings		
2a Security Classification Authority		3 Distribution Availability of Report		
2b Declassification Downgrading Schedule		Approved for public release; distribution is unlimited.		
4 Performing Organization Report Number(s)		5 Monitoring Organization Report Number(s)		
6a Name of Performing Organization Naval Postgraduate School	6b Office Symbol (if applicable) 55	7a Name of Monitoring Organization Naval Postgraduate School		
6c Address (city, state, and ZIP code) Monterey, CA 93943-5000		7b Address (city, state, and ZIP code) Monterey, CA 93943-5000		
8a Name of Funding Sponsoring Organization	8b Office Symbol (if applicable)	9 Procurement Instrument Identification Number		
8c Address (city, state, and ZIP code)		10 Source of Funding Numbers		
		Program Element No	Project No	Task No	Work Unit Accession No

11 Title (include security classification) A STUDY OF PC-BASED HF IONOSPHERIC PROPAGATION PREDICTIONS FOR USE IN NAVAL COMMUNICATIONS

12 Personal Author(s) Georgios H. Giakoumakis

13a Type of Report Master's Thesis	13b Time Covered From To	14 Date of Report (year, month, day) June 1990	15 Page Count 64

16 Supplementary Notation The views expressed in this thesis are those of the author and do not reflect the official policy or position of the Department of Defense or the U.S. Government.

17 Cosati Codes			18 Subject Terms (continue on reverse if necessary and identify by block number)
Field	Group	Subgroup	High Frequency (HF) Ionospheric Propagation

19 Abstract (continue on reverse if necessary and identify by block number)

High frequency (HF) ionospheric propagation predictions have been available on mainframe computers since the late 1960s. Since the advent of low cost, computationally powerful personal computers, several propagation codes have been ported from mainframes to PC's. This study compares results from two versions of the IONCAP and PROPHET HF propagation prediction codes to a database of measured electric field strengths.

IONCAP-PC 2.5 predictions were compared to IONCAP-VAX 85.04 predictions and to those from PROPHET 3.2 (PC-version). A database of measured signal strengths from the CCIR containing over 16,000 points or cases was used as a benchmark for comparing code results.

For both IONCAP-PC 2.5 and PROPHET 3.2, field strength predictions were low in more than 50% of the cases examined. This was particularly true for PROPHET, which is considered to be a conservative model. PROPHET features quick solutions, graphical outputs, and a user-friendly environment, in comparison to IONCAP. IONCAP-PC 2.5, which is an improved version of a previous mainframe IONCAP, produced slightly more accurate predictions than IONCAP 85.04, and substantially better results than those from PROPHET.

20 Distribution Availability of Abstract ☒ unclassified unlimited ☐ same as report ☐ DTIC users	21 Abstract Security Classification Unclassified	
22a Name of Responsible Individual Richard W. Adler	22b Telephone (include Area code) (408)646-2352	22c Office Symbol ECAb

DD FORM 1473,84 MAR
83 APR edition may be used until exhausted
All other editions are obsolete
security classification of this page

A Study of PC-based HF Ionospheric
Propagation Predictions for Use in
Naval Communications

by

Georgios H. Giakoumakis
Lieutenant J.G., Hellenic Navy
B.S., Hellenic Naval Academy

Submitted in partial fulfillment of the
requirements for the degree of

MASTER OF SCIENCE IN ELECTRICAL ENGINEERING

from the

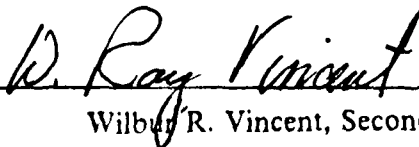NAVAL POSTGRADUATE SCHOOL
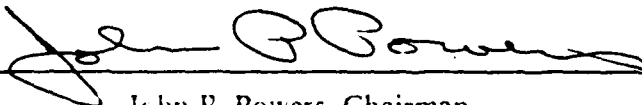June 1990

Author: _____

Georgios H. Giakoumakis

Approved by: _____

Richard W. Adler, Thesis Advisor

_____

Wilbur R. Vincent, Second Reader

_____

John P. Powers, Chairman,
Department of Electrical and Computer Engineering

ii

ABSTRACT

High frequency (HF) ionospheric propagation predictions have been available on mainframe computers since the late 1960s. Since the advent of low cost, computationally powerful personal computers, several propagation codes have been ported from mainframes to PC's. This study compares results from two versions of the IONCAP and PROPHET HF propagation prediction codes to a database of measured electric field strengths.

IONCAP-PC 2.5 predictions were compared to IONCAP-VAX 85.04 predictions and to those from PROPHET 3.2 (PC-version). A database of measured signal strengths from the CCIR containing over 16,000 points or cases was used as a benchmark for comparing code results.

For both IONCAP-PC 2.5 and PROPHET 3.2, field strength predictions were low in more than 50% of the cases examined. This was particularly true for PROPHET, which is considered to be a conservative model. PROPHET features quick solutions, graphical outputs, and a user-friendly environment, in comparison to IONCAP. IONCAP-PC 2.5, which is an improved version of a previous mainframe IONCAP, produced slightly more accurate predictions than IONCAP 85.04, and substantially better results than those from PROPHET.

TABLE OF CONTENTS

LIST OF FIGURES

vii

I. INTRODUCTION

Ionospheric propagation prediction programs are used daily in the Navy for HF communications planning. Therefore, an assessment of the usefulness and accuracy of these programs is needed. In order to accomplish this, measured values must be compared with values calculated from the propagation prediction programs. Typically, three parameters can be compared:

a. Maximum Usable Frequency (MUF),

b. Signal-to-noise ratio (S N) at the receiver input terminals,

c. Signal field strength at the receiver location.

Measured and calculated MUFs have been compared in the past. Fortunately, the MUF is a preliminary parameter that is used for more complex calculations.

Field strength comparisons between measured and calculated values are more popular than S N comparisons, since estimating noise levels is not involved.

In the real world during the propagation of a wave through the ionosphere, the following happens: There are numerous propagation paths possible between a transmitter and a receiver, depending on the vertical beamwidth of the transmitter's antenna and the ionospheric layers. Even though a radio wave enters the ionosphere with a certain angle, it is split into two components (ordinary and extraordinary) because of the presence of the earth's magnetic field. Conditions in the ionosphere are not identical for the two components. Their reflections take place at different altitudes and their delay times, polarization and losses are different. They are also received at different in-coming angles at the receiver. Therefore, more than one signal arrives at the receiver at the same time. Each one has different amplitude, phase and polarization. Calculation of signal field strength at the receiver is a very complicated process due to all of these factors.

In order for the existing prediction programs to simulate the propagation through the ionosphere, the following are assumed:

1. There is no interference between signals transmitted by the same source that arrive at the receiver through different paths;

2. There is no birefringence (wave component splitting);

3. The wave's polarization does not change by passing through the ionosphere, or after ground reflection and;

4. There is no layer fluctuation during propagation.

1

A. HISTORICAL BACKGROUND

For many years, numerous organizations have used the HF spectrum to communicate over long distances. In the late thirties, communication systems were subject to large variations in performance. Effectiveness of long-distance systems increased in proportion with the ability to predict variations in the ionosphere, since such an ability permitted the selection of optimum frequencies and other circuit parameters. To measure ionospheric parameters, a worldwide network of ionosondes was established. Variations in signal amplitudes were observed and then recorded over various HF paths. Worldwide noise measurements were also taken. The results of this research showed that most of the variations in HF path performance were directly related to changes in the ionosphere, which in turn were affected by solar activity, seasonal and diurnal variations. Latitude and longitude of the transmitter and the receiver also influenced performance.

By 1948 a treatise of ionospheric radio propagation was published by the Central Radio Propagation Laboratory (CRPL) of the National Bureau of Standards, which outlined the state-of-the-art in HF propagation. Manual techniques were given for analyzing HF circuits of short, intermediate, and long distances. [Ref. 1]

Because these manual techniques were laborious and time consuming, various computer programs were developed to predict HF circuit performance. All these programs were based on manual methods and used various numeric representations of the ionospheric data.

From 1945 to 1960, the Radio Propagation Laboratory (RPL) of the U.S. Army collected data concerning monthly median receiver input voltages for several circuits in the HF band. This data was statistically analyzed in order to study the parameters that influence propagation through the ionosphere, and a number of reports presented engineering methods of evaluating sky-wave field strengths [Ref. 2].

Recently, another bank of field strength data, called the CCIR HF data bank, was collected. This data bank contains 16,268 data points of observed electric field strength correlated with information for the month, year, hour (UT), frequency, and sunspot number and includes 181 combinations of circuit and frequency. The frequencies are from 2.5 to 26 MHz, path lengths are between 175 and 26,000 km, and the data spans the period of 1964 to 1985 for two sunspot cycle variations.

The median monthly skywave electric field strength (observed) is in one-hour time blocks. Its value is given in dB relative to $1 \mu V$ m for a 1 kW ERP source.

Professor A. Tomko from Johns Hopkins University used this data bank to make a statistical analysis of the prediction accuracy of HF propagation models [Ref. 3]. One

2

of the models that he analyzed was IONCAP, mainframe version 85.04 [Ref. 4]. The results of his analysis will be used to compare with other models. In order to make an evaluation he compared each model's predictions of the electric field strength. E_p, with empirical data, E_o, from the CCIR IIF data bank, by computing the prediction error,

$\varepsilon = E_p - E_o$.

B. ANALYSIS

In the next chapters, data from the same CCIR data bank will be used, and the same methodology that was mentioned above will be followed to analyze the performance of IONCAP-PC 2.5 and PROPHET.

First, the two versions of IONCAP will be compared and then IONCAP-PC 2.5 with PROPHET. Finally, an evaluation of IONCAP-PC 2.5 and PROPHET will be conducted for paths, defined as polar. The appendix also contains a short analysis of another IIF propagation model, called MINIPROP.

II. THEORETICAL BACKGROUND

A. SKY WAVE PROPAGATION

Sky wave propagation is defined as radio wave reflections in which ionospheric reflections dominate over other mechanisms.

1. The Ionosphere

a. Structure

The ionosphere consists of several electrically conducting layers above the Earth's surface which play a very important role in the propagation of radio waves. Radiation from the sun is the primary source of ionization of these layers and controls their intensity. The ionization rate at various altitudes depends upon the intensity of the solar radiation and the ionization efficiency of the neutral atmospheric gases. Since the sun's radiation is progressively absorbed in passing through the atmosphere, the residual ionizing ability depends upon the length of the atmospheric path, and consequently upon the solar zenith angle. The maximum ionization rate occurs when the solar zenith angle is zero, but geographic, diurnal and seasonal variations in ionization density also occur.

The ionosphere is divided into three layers, designated D, E, and F, respectively. These layers may be subdivided. From the viewpoint of HF propagation, the E-and F-layers act mainly as radio wave reflectors and permit long range propagation between terrestrial terminals. The D-layer acts mainly as an absorber causing attenuation in the lower HF range.

b. D-layer

The D-layer, at an altitude of 50-90 km above the earth, is the lowest layer. Its electron density exhibits large diurnal variations. The D-layer appears after sunrise and attains its maximum value shortly after local solar noon. It then gradually breaks down, and disappears after sunset. There is also a seasonal variation with maximum values during summer. Short waves penetrate the D-layer, but they are attenuated while passing through the layer.

c. E-layer

The E-layer, at 90-130 km, is subdivided into "normal" and "sporadic" layers. The former has its maximum electron density at 110 km altitude. It displays a strong solar zenith angle dependence with maximum density near noon and a seasonal

maximum in summer. It also displays a solar cycle dependence with maximum density at solar sunspot maximum. The normal E-layer is important for daytime HF propagation at distances less than 2000 km.

The E_s is known as the sporadic E-layer because it arises only occasionally at most latitudes. It is located 120 km above the Earth and, when present, causes higher than normal critical frequencies. Its occurrence is strongly latitude dependent. At high latitudes, it is essentially a night-time phenomenon; at low latitudes, a daytime phenomenon.

d. F-layer

The F-layer extends upwards from about 130 km and is divided into the F1- and F2-layers. The F1-layer exists only during daylight hours and is located 170 to 220 km above the earth. The F2-layer is located 225 to 450 km above the earth and usually exhibits the highest electron density, which ranges from 10^{12} electrons/m^3 in daytime, to about 5×10^{10} electrons/m^3 at night. The F2-layer cannot be described by a simple model since it is strongly influenced by winds, diffusion and other dynamic effects. It is the principal reflecting layer used for long-distance communications. Its height and ionization density vary diurnally, seasonally and over the sunspot circle. At night, the F1-layer merges with F2-layer at a height of about 300 km.

2. Maximum Usable Frequency

Predicting the performance of an HF skywave path is a complex problem. However, there is much that can be learned from examining the dependencies of some of the relevant characteristics, of which the maximum usable frequency is particularly important.

The maximum usable frequency (MUF) for any transmission distance is calculated from the critical frequency multiplied by a factor that is a function of the transmission distance (Figure 1 on page 6). In practice, the MUF is not a sharp limit since some propagation is possible on frequencies greater than the MUF. This happens since neither the ground nor the ionosphere are smooth reflectors.

The critical frequencies of the E- and F2-layers, known as f_cE and f_cF2 respectively, are the highest frequencies that can be reflected from the two layers at vertical incidence with the ionosphere; they are related to the maximum electron densities in those layers. The value of f_cF2 is usually greater than the value of f_cE because the electron concentration in the F-layer is usually greater than in the E-layer.
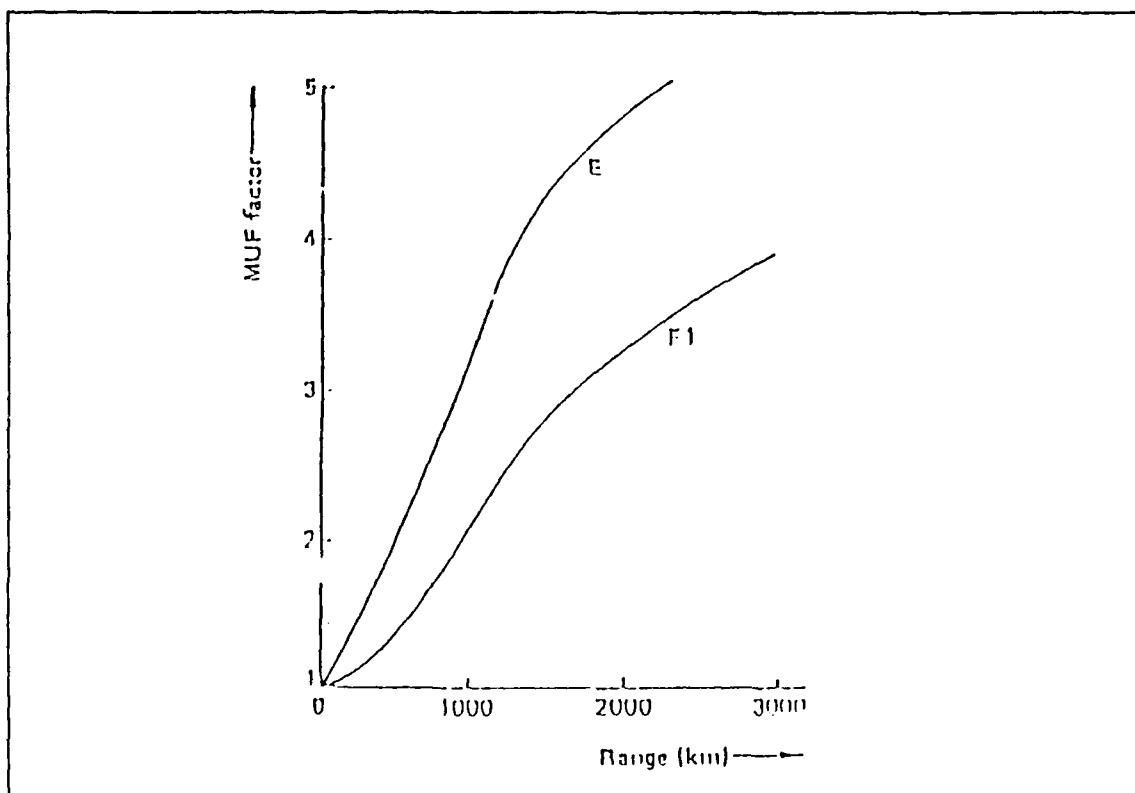
Figure 1.   Range dependence of MUF factor for E- and F-layers. From [Ref. 5: p. 64].

The plasma frequency f_N is given by

$$f_N = 9N^{0.5},\qquad(2.1)$$

where N is the electron density in electrons per cubic meter and f_N is in Hertz. If N_m is the maximum electron density in a given layer, then all waves for frequencies less than the plasma frequency that enter the ionosphere at vertical incidence will be reflected back to earth. The critical frequency is given by

$$f_o = 9N_m^{0.5}.\qquad(2.2)$$

a.   Variation of the critical frequency

(1)   Solar Cycle dependence.   Figure 2 on page 8 shows the monthly mean noon critical frequencies of the E- and F2-layers over the last solar cycle. It can be seen

6

that there is a correlation of the F2-layer critical frequencies with the eleven-year solar cycle.

Additionally, the seasonal variation of f_oE is in phase with solar zenith angle (greater in the summer months). In contrast, the seasonal variation of f_oF2 is in antiphase with solar zenith angle. This is known as the "winter anomaly". Therefore, unlike the E- and the F1-layer, the F2-layer does not follow a simple solar zenith angle either diurnally or seasonally.

(2) Annual, Seasonal, and Diurnal variations. There is an annual variation of the monthly median f_oF2 . The greatest variation over the solar cycle for daytime conditions occurs in winter and the least variation in the summer. By contrast, night-time conditions in the winter are mostly unaffected by sunspot number.

There is a seasonal variation of the monthly median f_oF2. The largest variation over the year occurs during periods of high sunspot activity.

There is also a diurnal variation of the monthly median f_oF2. Diurnal variations are most marked during winter months.

3. Path Attenuation and Attainable Field Strengths

For a specific shortwave path, when determining the transmitter power and antenna gains, the calculations are based on stable properties of the path. With propagation conditions continuously varying, these path properties are characterized by attenuation and field strength values that can be expected for a given percentage of the time.

a. Losses in a shortwave system

If a shortwave link is considered as a closed transmission system, starting with the transmitter output and ending with the receiver input, its total losses L_{syst} can be given from the following individual losses:

$$L_{syst} = L_{Fr} + L_I + L_B + Y_F - G_s - G_E \qquad (2.3)$$

where

L_{Fr} is the free-space attenuation in dB,

L_I is loss in the ionosphere in dB,

L_B is loss from ground reflections in dB,

Y_F is a fading reserve in dB, and

G_s and G_E are the gains of the transmitting and the receiving antennas in dB, respectively.
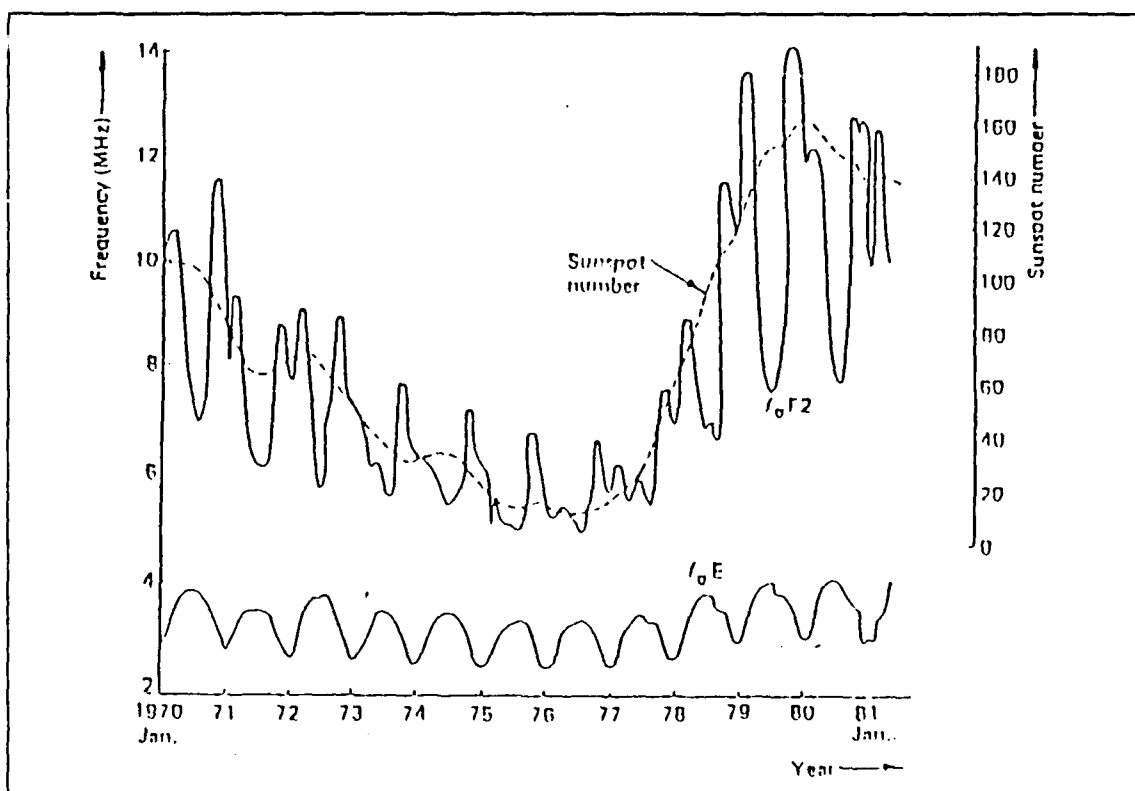
Figure 2. Solar dependence of the critical frequency: Monthly mean of the noon critical frequencies observed at Slough 1970-81 with superimposed sunspot activity. From [Ref. 5: p. 68].

(1) Free space attenuation. The decrease in radiated power density from a transmit antenna is a function of the square of the distance, with field strength decreasing linearly with distance. Considering isotropic radiators for transmitting and receiving, free space attenuation is given in dB from the relation:

$$L_{Tr} = 20 \log(4\pi d_{eff}/\lambda) = 32.44 + 20 \log f + 20 \log d_{eff} \qquad (2.4)$$

where f is the operating frequency in MHz and d_{eff} is the effective path length in km.

(2) Ionospheric losses. Radiowaves passing through the ionosphere suffer from loss due to absorption in the D-layer. This loss depends on the zenith angle of the sun, ψ, and the sunspot number R.

8

The absorption index is given from the relation:

$$I = (1 + 0.0037R)(\cos 0.881\psi)^{1.3} \tag{2.5}$$

The absorption index is higher during winter months than during the rest of the year, therefore, correction factors are used to account for the winter anomaly.

The loss also depends on the elevation angle of the radiation and the effective frequency $f + f_H$. The effective frequency is the sum of the operating frequency and the gyrofrequency f_H. The gyrofrequency is created by the Earth's magnetic field ($f_H = 2.84 \times 10^{10} \times B$ where B is the magnetic induction in Wb m^2) .

With absorption index, the effective frequency $f + f_H$, and the angle of elevation, the loss in the ionosphere L_l can be determined with the aid of the nomogram in Figure 3 on page 10.

(3) *Ground reflections loss.* If a sky wave is reflected by the ionosphere back to earth, it reaches the ground with a polarization differing from that of the emitted wave. The energy of the incident wave will be split into vertical and horizontal components. Assuming that these two components are equal, the reflection loss from the ground, in dB.

$$L_B = 10 \log(\frac{R_v^2 + R_h^2}{2}) \tag{2.6}$$

where R_v is the reflection coefficient of the vertical component and R_h is the reflection coefficient of the horizontal component.

(4) *Fading reserves.* The losses described thus far refer to a stable radio path. However, field strength at the receiving point is influenced by continuously fluctuating propagation conditions along the path, due to several types of fading phenomena. The probability of occurrence of a specific field strength value follows a Rayleigh distribution. A fading reserve of 14 dB is, in general, recommended for shortwaves in order to attain availability 90% of the time.

Example: Angle of elevation $\vartheta = 8°$, absorption index $I = 1.08$. The line (1) connecting these two values intersects with the reference line at point P. The connecting line (2) for the frequency 22.2 MHz through P shows a loss of 6 dB per hop.
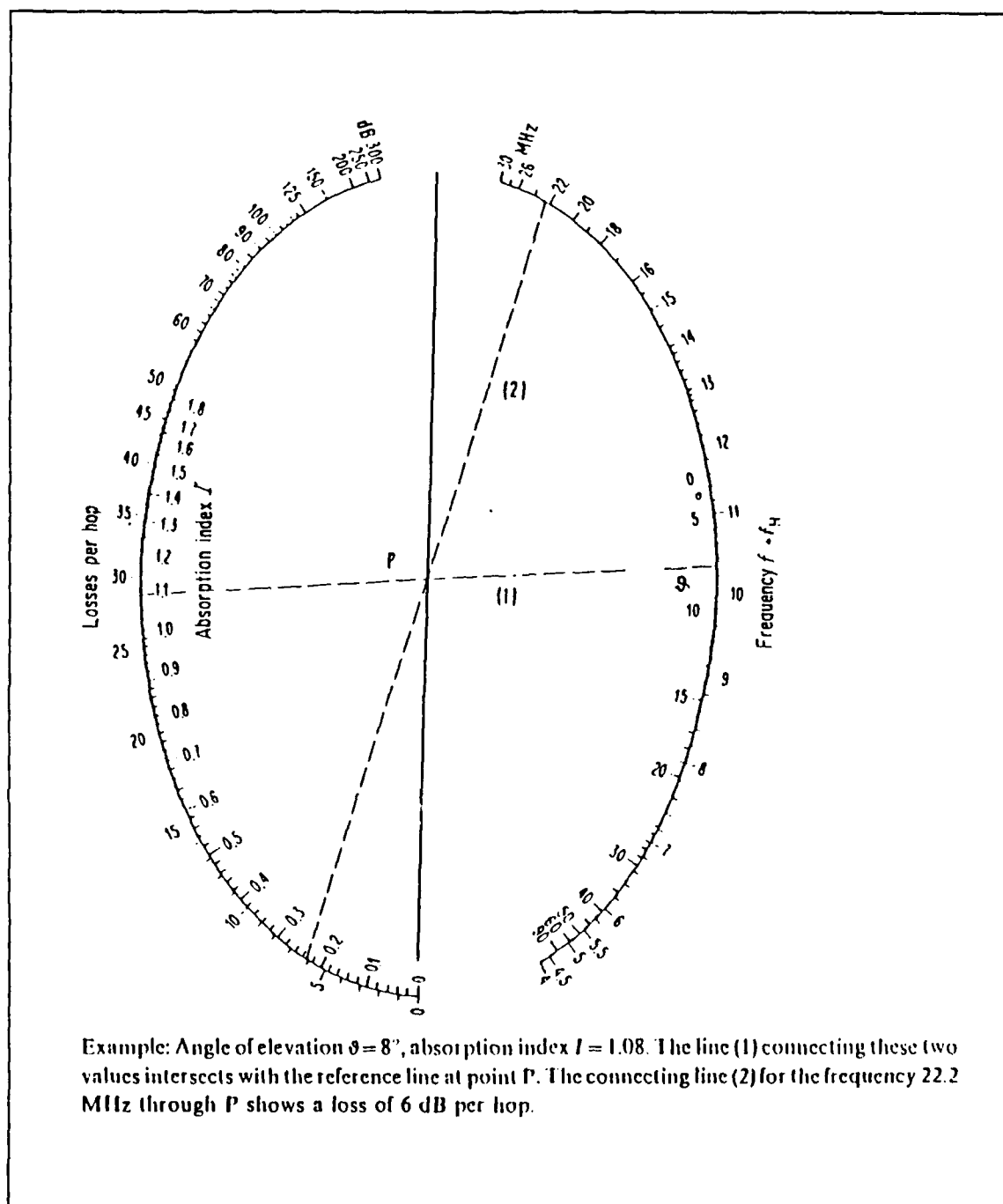
Figure 3. Nomogram for determining the ionospheric losses per hop as a function of the absorption index, the elevation angle and the effective frequency. From [Ref. 6: p. 217].

10

III. MODEL DESCRIPTIONS

A. IONCAP

The Ionospheric Communications Analysis and Prediction Program (IONCAP) is a program that attempts to solve the physics of each parameter [Ref. 7]. Therefore, its solutions are accurate but computationally intensive. For this reason, IONCAP is often used for communication circuit planning.

IONCAP was designed in modular form, therefore, any subsection can be replaced without affecting the rest of the program and is written in FORTRAN. The program is divided into seven independent subroutines:

1. Input
2. Path geometry
3. Antennas
4. Ionospheric parameters
5. Maximum usable frequency
6. System performance
7. Output.

Input subroutines handle various input options. Three kinds of input are: card image, a long term data tape image, and an antenna tape image. Path geometry subroutines determine circuit geometry, select optimum areas to sample the ionosphere, and evaluate the magnetic field at these sample areas. Antenna subroutines process antenna data input cards and calculate antenna gains.

Ionospheric parameter subroutines evaluate all ionospheric parameters needed by the program. A complete explicit electron density profile is used in this program. The profile includes a D-E layer, an F2-layer, an F1-ledge and an E-F valley.

Maximum Usable Frequency (MUF) subroutines evaluate MUFs and Optimum Traffic Frequencies (FOTs). The method used is a direct evaluation of the frequency that propagates 50% of the time for the MUF and 90% of the time for the FOT. The E-, F1- and F2-layer MUFs are computed. The sporadic-E MUF is also computed.

System performance subroutines evaluate all the needed circuit parameters. There are two different sets of subroutines, one for shorter distances (less than 10,000 km) and one for longer distances. However, the user may run either set of subroutines for any given distance (overriding the 10,000 km breakpoint).

The short path model evaluates each possible ray path for the circuit; high and low angle, E, F1, and F2 modes, over the MUF modes and sporadic-E modes. Losses include regular D-E absorption and sporadic losses. For lower frequencies which have low reflection heights (less than 90 km), a correction to the frequency dependence parameter was added.

By using the antenna gains and the ionosphere-loss function, the model evaluates the optimum radiation angle at the transmitter and the optimum reception angle at the receiver. The 29 output subroutines generate all output options as line images.

The IONCAP program performs four basic analysis tasks. These tasks are summarized below:

1. Ionospheric Parameters

The ionosphere is predicted by using parameters which describe the four ionospheric layers: E, F1, F2, and E_s. At each sample area the location, time of day, and all ionospheric parameters are derived. These can be used to find an electron density profile. By integration, a plot of reflection height against frequency can be constructed, which is called an ionogram.

2. Antenna Patterns

The user may precalculate the antenna pattern and gain used for system performance predictions.

3. Maximum Usable Frequency (MUF)

The maximum frequency at which a skywave mode exists can be predicted. The 90% (FOT), 50% (MUF), and 10% (Highest Probable Frequency) levels are calculated for each of the four ionospheric layers. These numbers are a description of the state of the ionosphere between two locations and not a statement on the actual performance of any operational communication circuit.

4. System Performance

A comprehensive prediction of radio system performance parameters (up to 22) is provided.

B. PROPHET

The Advanced PROPHET HF prediction is the follow-on successor to the SOLRAD PROPHET family of real-time HF propagation prediction and assessment systems [Ref. 8 and 9]. It has been designed to give conservative and real-time solutions, in order to support US military tactical communications.

In order to achieve this. PROPHET does not attempt to solve the physics of each parameter, like most of the classical HF prediction models do. PROPHET solves the problem by using simplified empirical models which have been thoroughly verified with HF oblique incidence data (ionograms). This provides rapid solutions with small and less expensive computers.

The Advanced PROPHET system consists of over 24 ionospheric algorithms and several special application models.

The basic model set used in Advanced PROPHET is contained in a module called "PROFLIB". This module calculates the various parameters, like the MUF, and then applies them to an application routine which produces the final product.

The first quantity needed for a given skywave channel is the channel bandwidth or frequency spread between the MUF and the Lowest Usable Frequency (LUF). An algorithm known as MUF-85 has been developed in order to calculate the MUF. A comparable algorithm to calculate the LUF also has been developed. The LUF model is complicated by absorption effects.

On several of the PROPHET products, an additional frequency, the Frequency of Optimum Transmission (FOT), is noted. The FOT is defined as the frequency with 90% reliability, and is given as a guide to the user in selecting the optimum frequency for the current mission.

The bandwidth for a given channel depends primarily on solar effects in the ionosphere. However, communicating information over this channel depends not only on the frequency, but also on various enviromental effects such as noise, absorption, required signal-to-noise ratio for the class of emission and antennas. A model for the expected noise for various environments has been developed. It includes contributions from atmospheric, galactic and man-made sources. An algorithm calculates the ionospheric absorption index for any time and location. System parameters and antenna patterns are input to PROPHET by the user. An algorithm converts geographic coordinates to range between transmitter and receiver and azimuth beam headings.

An algorithm computes the ray paths that will propagate between the designated transmitter and receiver, for the specified operating frequency and for a specific model of the ionosphere. The calculations are controlled by the initial launch angle, launch angle increment, and maximum launch angle used in computing the ray paths. The calculations start with the initial angle and compute successive rays for angles increased by an increment until two rays are found that bracket the receiver site. An interpolation routine is then used to find the launch angle that will hit the receiver. The resulting ray

13

path is called a mode. The procedure continues until the launch angle reaches the maximum limit or the number of specified modes is reached. Influences by a jammer site are included, and models are used to assess the effects they have on the receiving system.

Short-range propagation by ground or surface wave depends on several factors such as frequency, antenna height, ground conductivity, dielectric constant, and polarization. Empirical models are used to simulate this propagation.

The field strength model was derived by comparing the output of the model with an extensive set of measurements which depends on the MUF, LUF, the effective radiating power and environmental parameters. It provides a method for rapid assessement of HF skywave signal quality as a function of frequency within the propagation bandwidth for links between specified points on the Earth's surface. It also provides matrices of the signal-to-(noise + jammer) ratio as functions of time and frequency.

The above models comprise the basis for HF modeling, as expressed in PROPHET.

IV. COMPARISON OF IONCAP 85.04 WITH IONCAP-PC 2.5

A. ASSUMPTIONS

Statistical analysis of the prediction accuracy of IONCAP 85.04 has been conducted by Professor A. Tomko and the results are contained in Reference 3. Comparison of IONCAP 85.04 predictions with CCIR HF data bank measurements encompassed all values (16,268) documented in the CCIR data bank. Values from IONCAP-PC 2.5, which is an improved version of IONCAP 85.04, were compared to a limited number of values from the CCIR data bank.

Three factors were considered that mainly influence the propagation through the ionosphere:

1. The Path Length

A short path was considered to be a path less than 2500 km. A medium path is a path greater than 2500 km but less than 8000 km. A long path is a path greater than 8000 km. The same classification of paths has been done in Reference 3. Therefore, short, medium, and long paths were chosen for IONCAP-PC 2.5 in the same proportion to the paths that were contained in the CCIR data bank.

2. The Season of the Year

The data were classified in two periods, winter and summer. Winter was considered October to March and summer from April to September for the northern hemisphere. For a fair sampling, the data was chosen in the same proportion as in the CCIR for these two periods.

3. The Sunspot Number

The sunspot number was an important factor for choosing the sample data. The CCIR data was sorted by category: long, medium, and short paths. Each category was then plotted versus the sunspot number. The samples were chosen so that their distribution versus sunspot number was similar to the distribution of the CCIR data but on a smaller scale.

The lines of the graphs, obtained from the analysis of IONCAP-PC 2.5, merely connect data points.

B. ANALYSIS

1. Macroscopic View of All Path Data

Figures 4 and 5 show the frequency distribution of the predicted errors for the two versions of IONCAP. The standard deviation of the error distribution of IONCAP-PC 2.5 is a bit smaller than the standard deviation of IONCAP 85.04. However, this does not imply better performance for IONCAP-PC 2.5 because the median of the error distribution for IONCAP 85.04 is closer to zero than the median error of IONCAP-PC 2.5.

Figures 6 and 7 show the cumulative distribution of the absolute value of prediction errors for the two versions of IONCAP. Comparing Figure 6 with Figure 7, it is seen that 85% of IONCAP-PC 2.5 data is included between -20 dB and + 20 dB error, while for IONCAP 85.04, only 80% of the data is included. Therefore, it is concluded that IONCAP-PC 2.5, in general, is slightly more accurate than IONCAP 85.04 for this measured data base.

In Figures 8 and 9, the frequency distribution of the prediction errors for the two versions of IONCAP is shown for various path lengths. Figures 10 and 11 show the cumulative distribution of the absolute value of the prediction errors for the two versions of IONCAP, for various path lengths. The peak values of the error frequency for IONCAP-PC 2.5 are higher (35%, 48%, and 31% for short, medium, and long paths respectively) than the respective peak values of IONCAP 85.04 (13%, 12.5% and 6.5%). The short path data represents 48% of all the data. The error value that corresponds to the peak value of error frequency for short path data is 7 dB for IONCAP-PC 2.5 and 2 dB for IONCAP 85.04. For long and medium path data, the error values that correspond to peak values of error frequency have no significant difference for the two versions of IONCAP. Therefore, because of the significant difference in error value of short path data, it is noted that, while there is such a significant difference in peak values of error frequency, there is not a significant difference in the final performance of the two different versions of IONCAP.

2. Paths Comparison

IONCAP 85.04 predictions are more accurate for short and medium paths than for long paths as shown in Figure 10. Figure 11 shows that for IONCAP-PC 2.5, predictions are a bit more accurate for short and medium paths than for long paths. For IONCAP 85.04 (Figure 10), it can be concluded that the random component of prediction error increases with increasing path length. The same cannot be said for
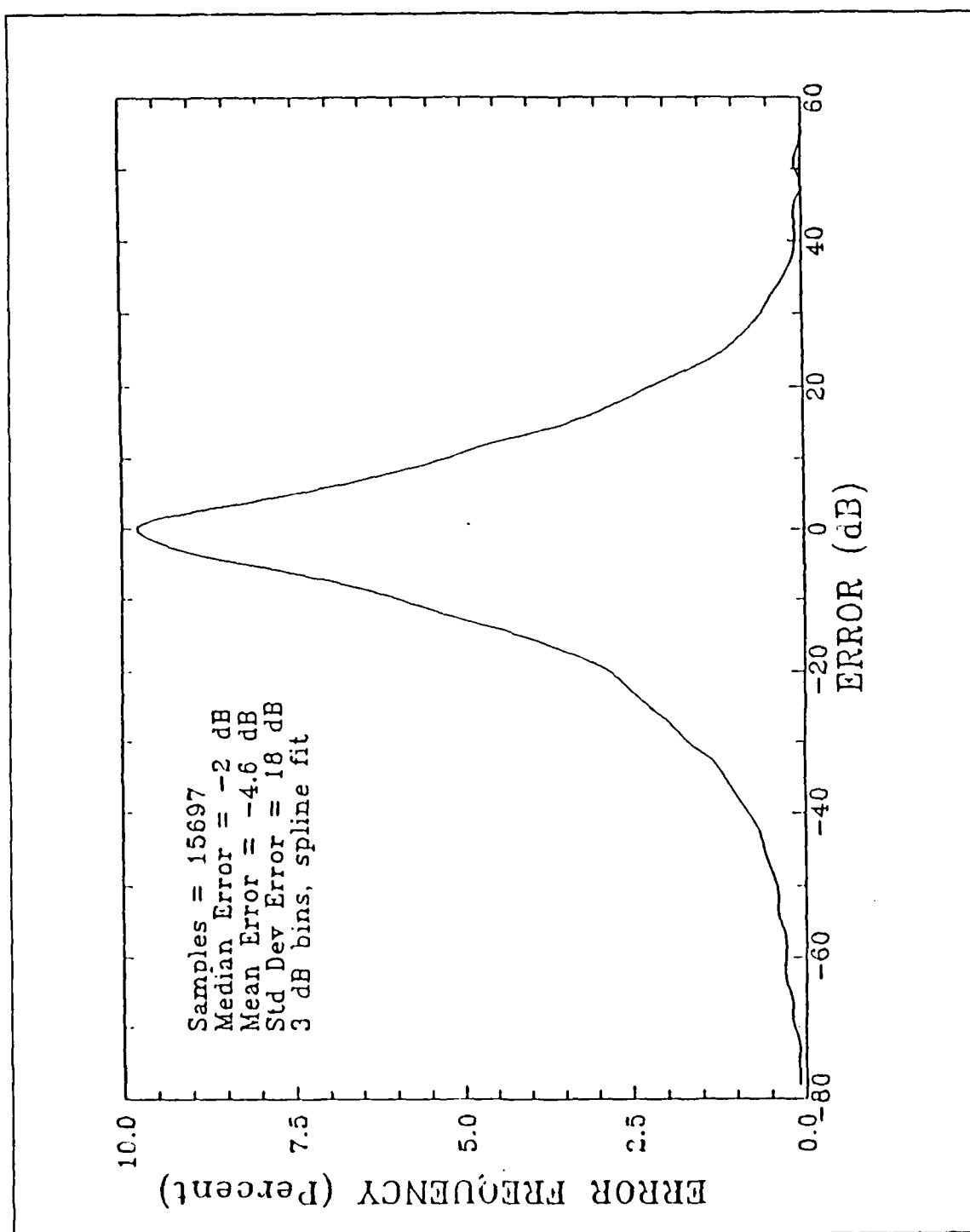
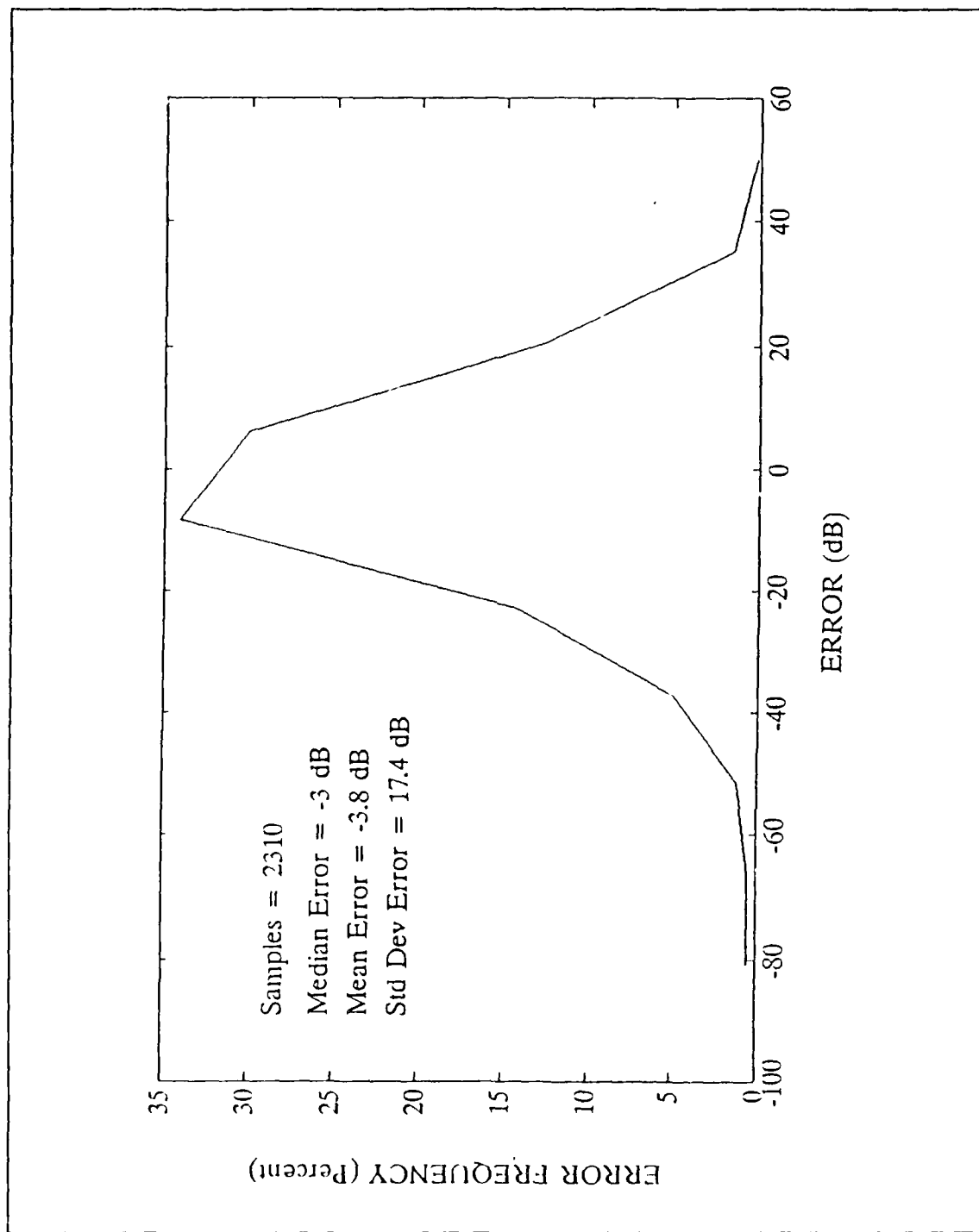Figure 4. Frequency distribution of IONCAP 85.04 prediction errors. From [Ref. 3].

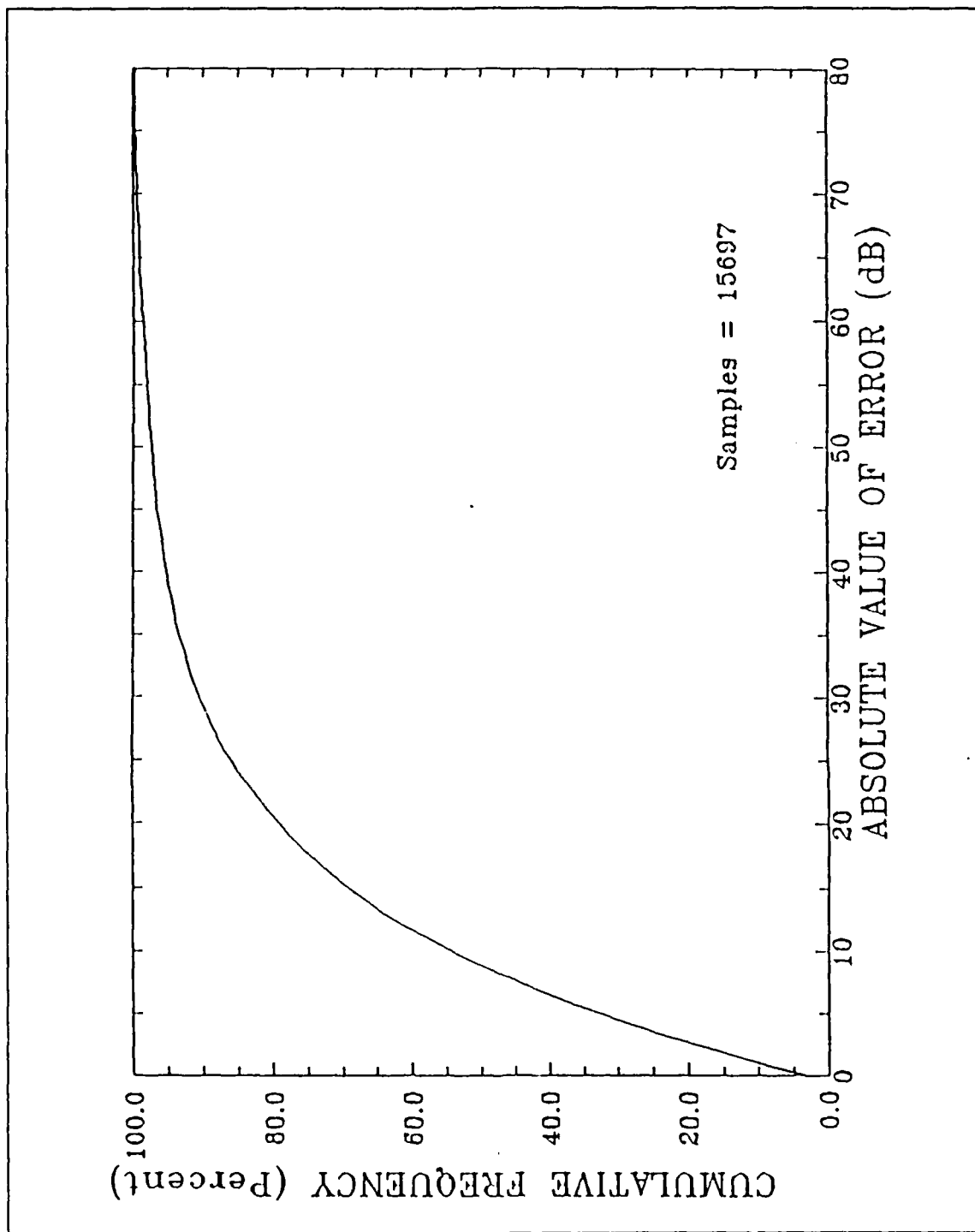Figure 5.   Frequency distribution of IONCAP-PC 2.5 prediction errors.

18

Figure 6. Cumulative distribution of the absolute value of IONCAP 85.04 prediction errors. From [Ref. 3].
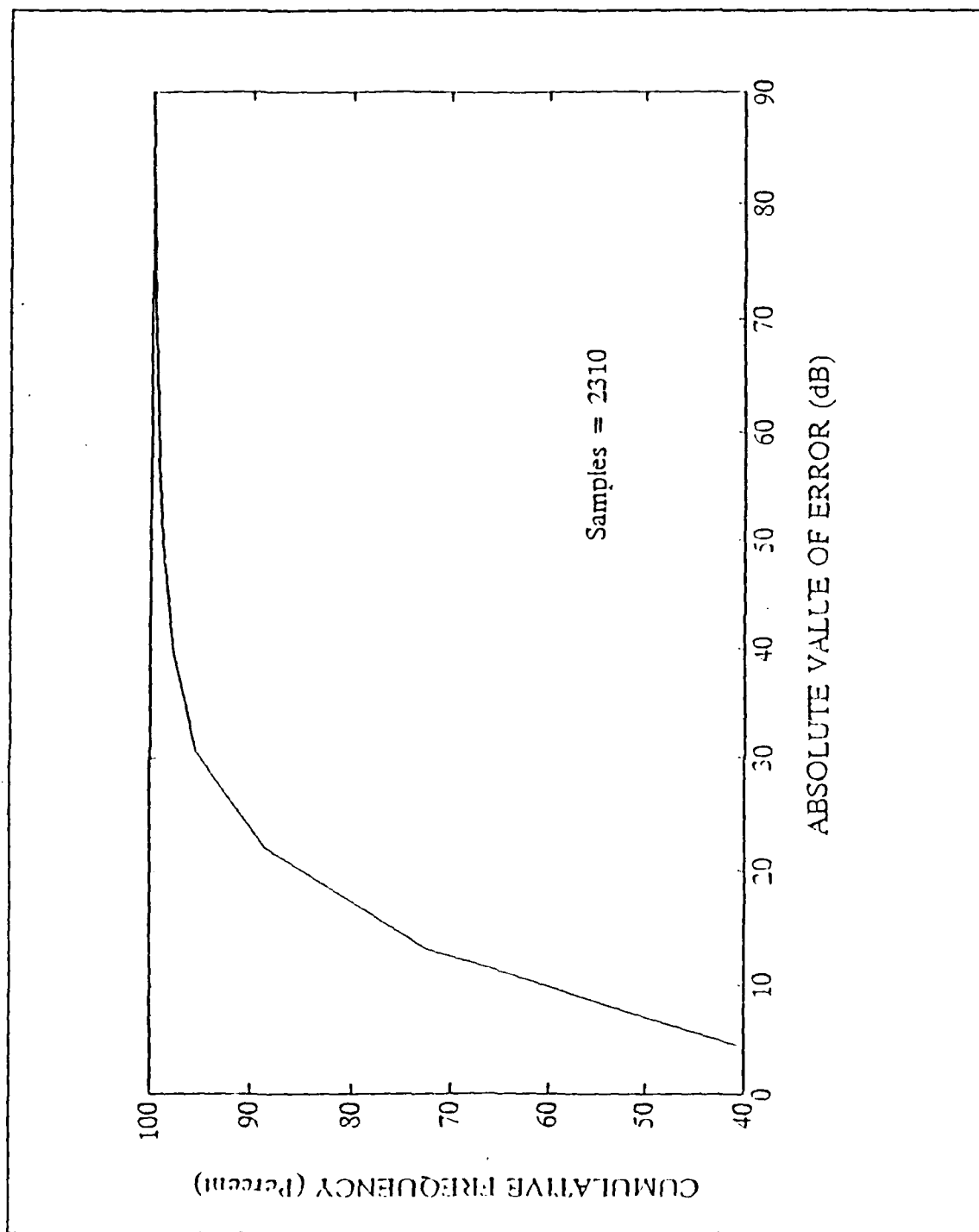
Figure 7.   Cumulative distribution of the absolute value of IONCAP-PC 2.5 prediction errors.
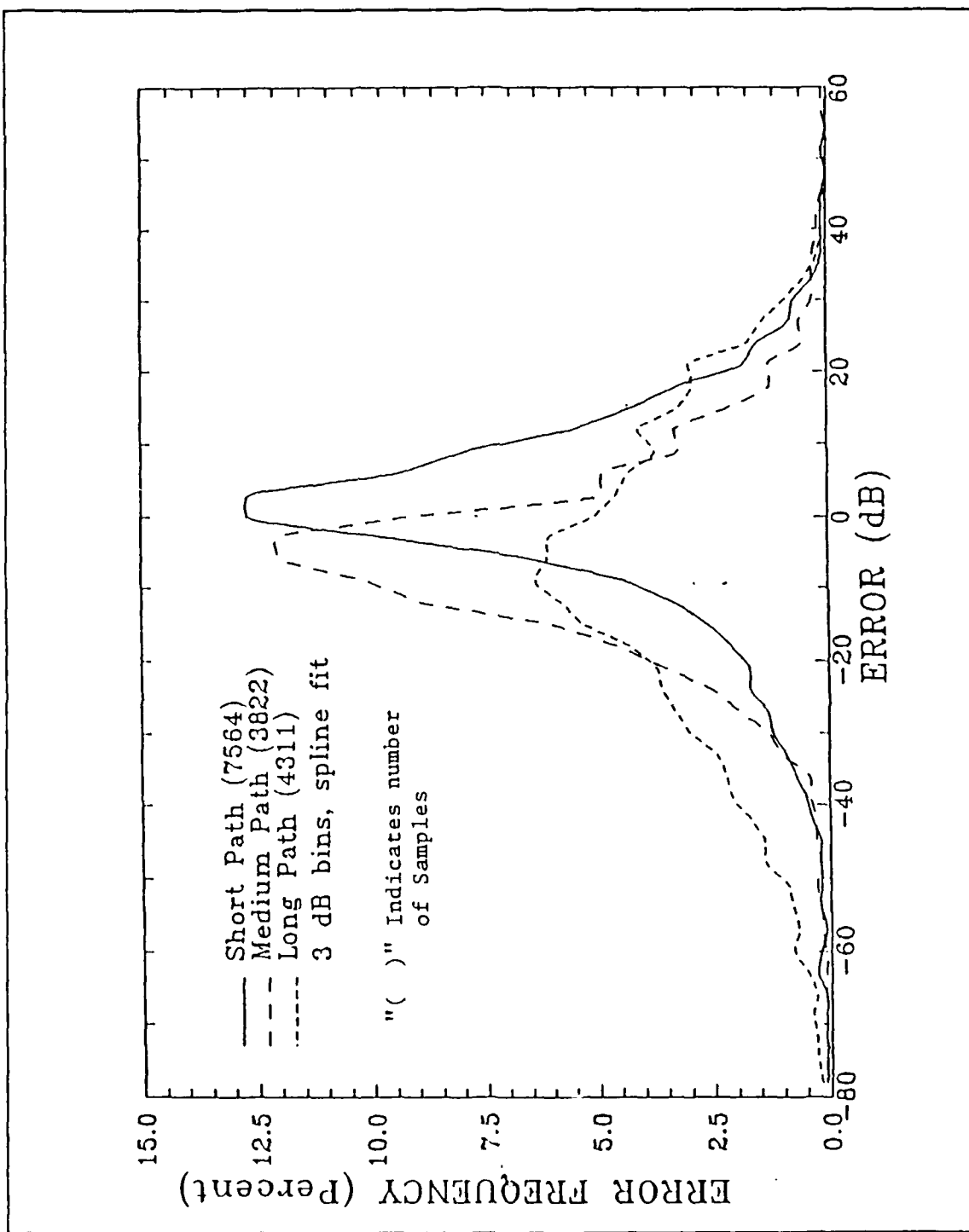
Figure 8.   Frequency distribution of IONCAP 85.04 prediction errors for various
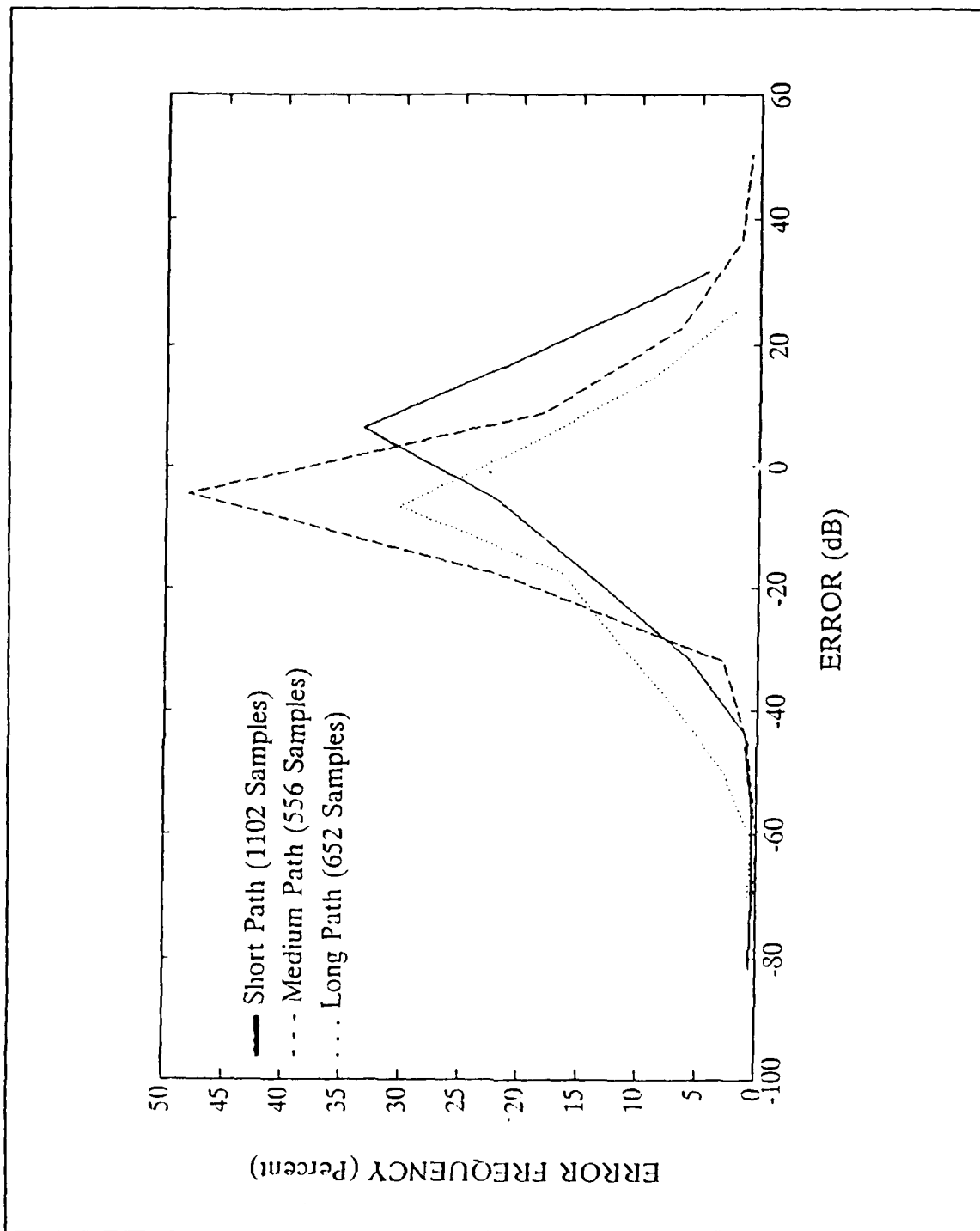path lengths. From [Ref. 3].

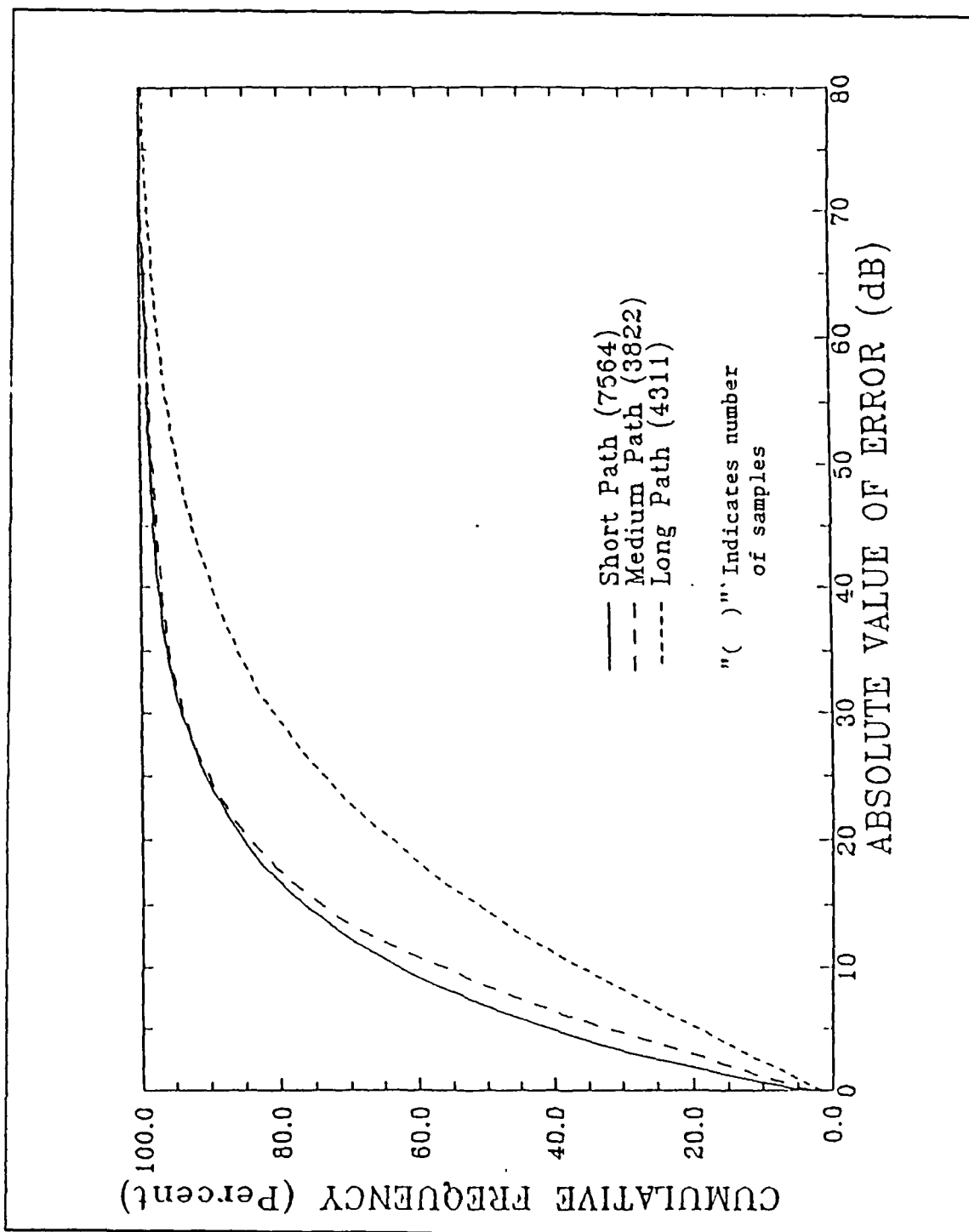Figure 9.   Frequency distribution of IONCAP-PC 2.5 prediction errors for various path lengths.

Figure 10.   Cumulative distribution of the absolute value of IONCAP 85.04 prediction errors for various path lengths. From [Ref. 3].
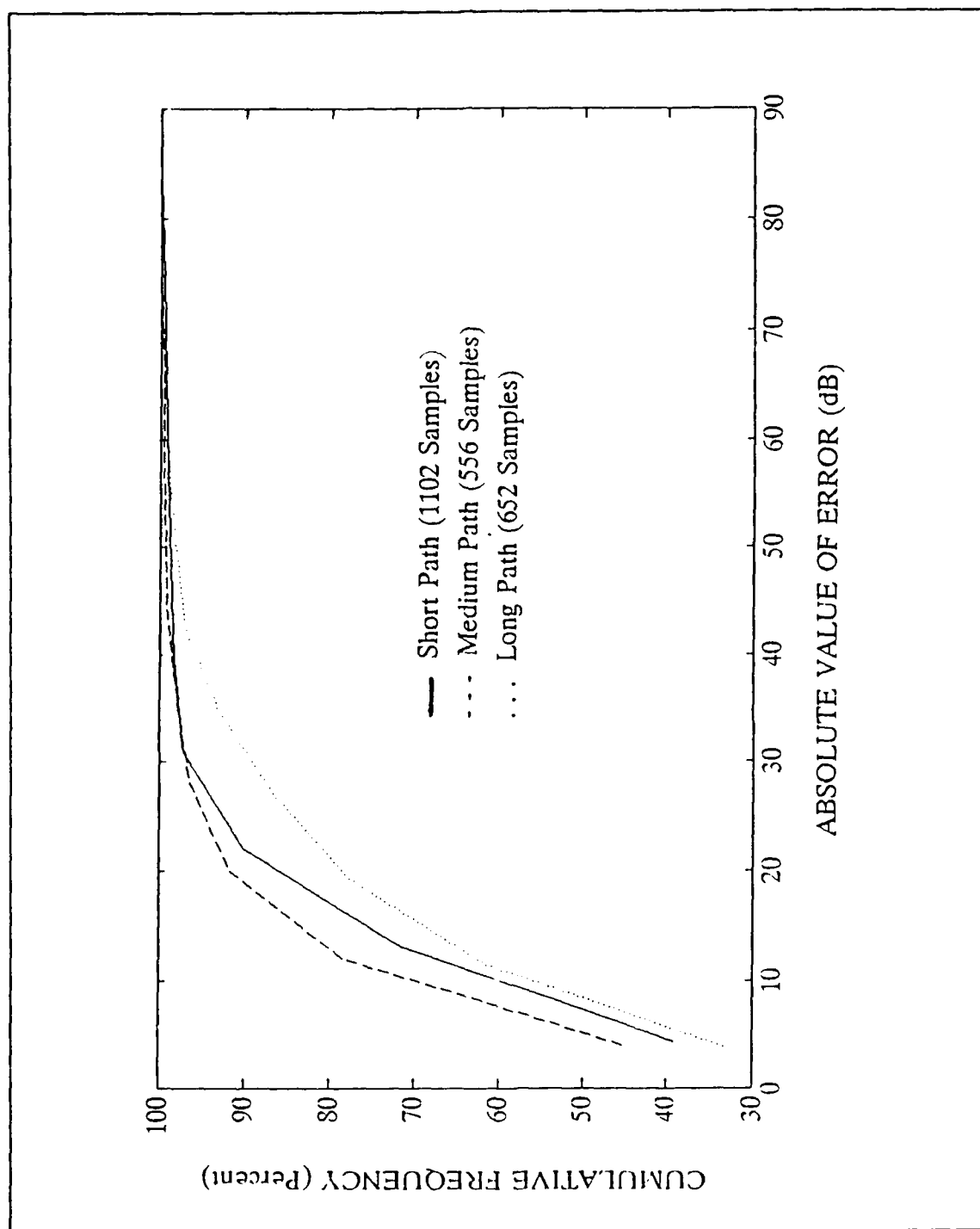
23

Figure 11. Cumulative distribution of the absolute value of IONCAP-PC 2.5 prediction errors for various path lengths.

IONCAP-PC 2.5 since the prediction error is less for medium paths than for short paths (Figure 11).

Figures 12, 13, and 14 show in detail, the statistics of the short, medium and long paths, respectively, for IONCAP-PC 2.5. These figures also reflect that field strength predictions for IONCAP-PC 2.5 are consistently low on medium and long paths, since the median error for both paths is negative (-6 and -8 dB respectively). The same conclusion is contained in Reference 3 for IONCAP 85.04.
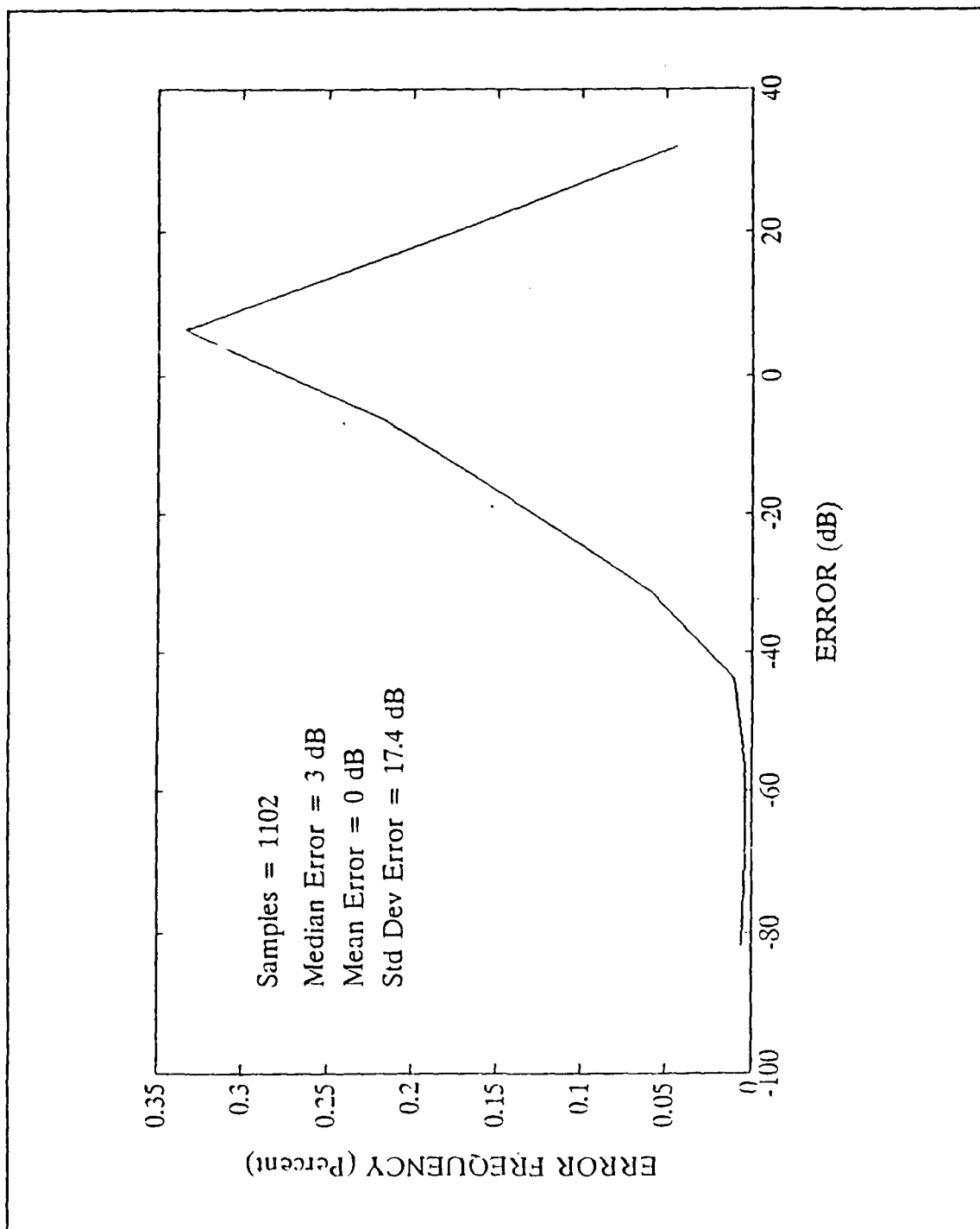
Figure 12. Frequency distribution of IONCAP-PC 2.5 prediction errors for short path lengths, for 1,102 samples.
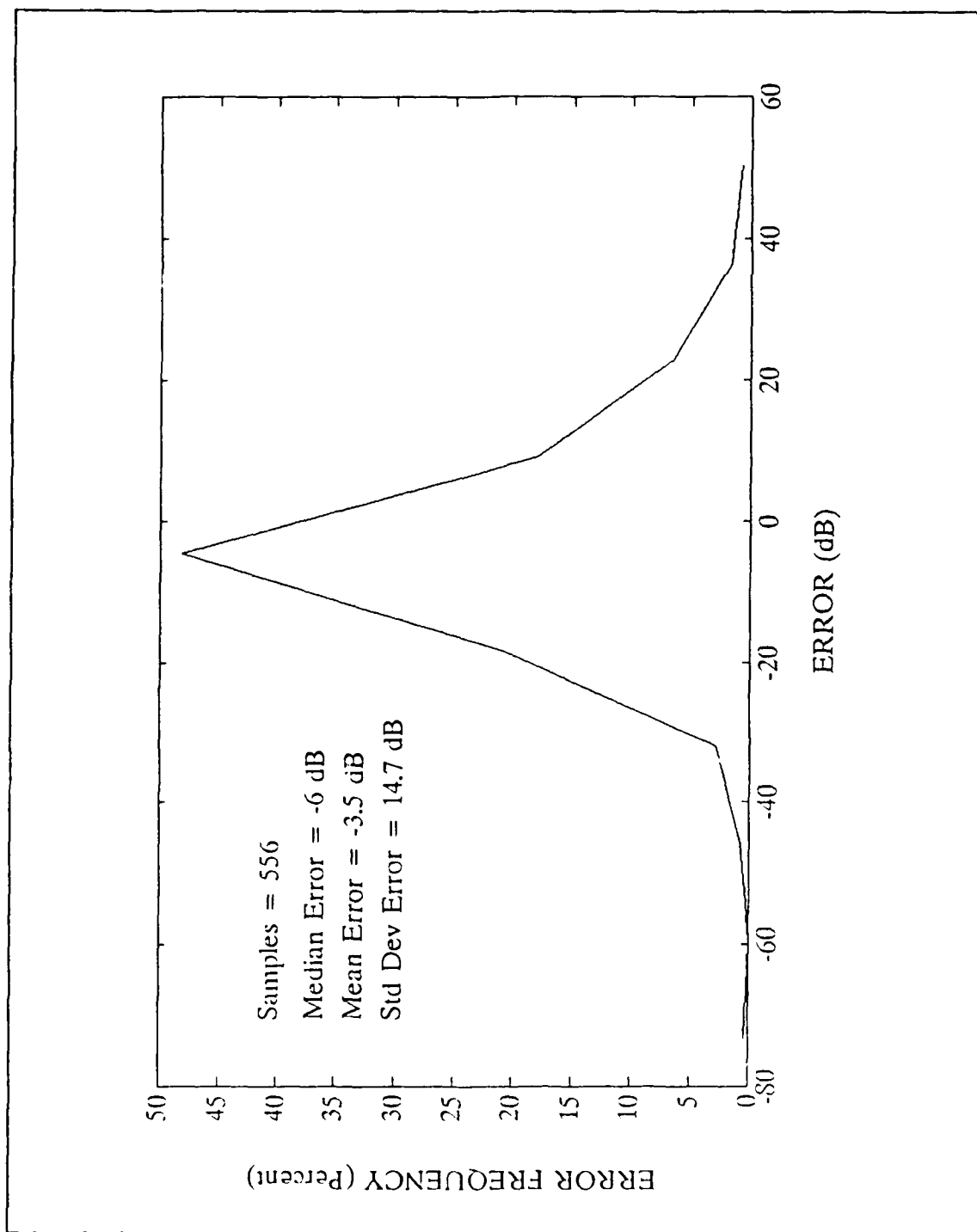
Figure 13. Frequency distribution of IONCAP-PC 2.5 prediction errors for medium path lengths.
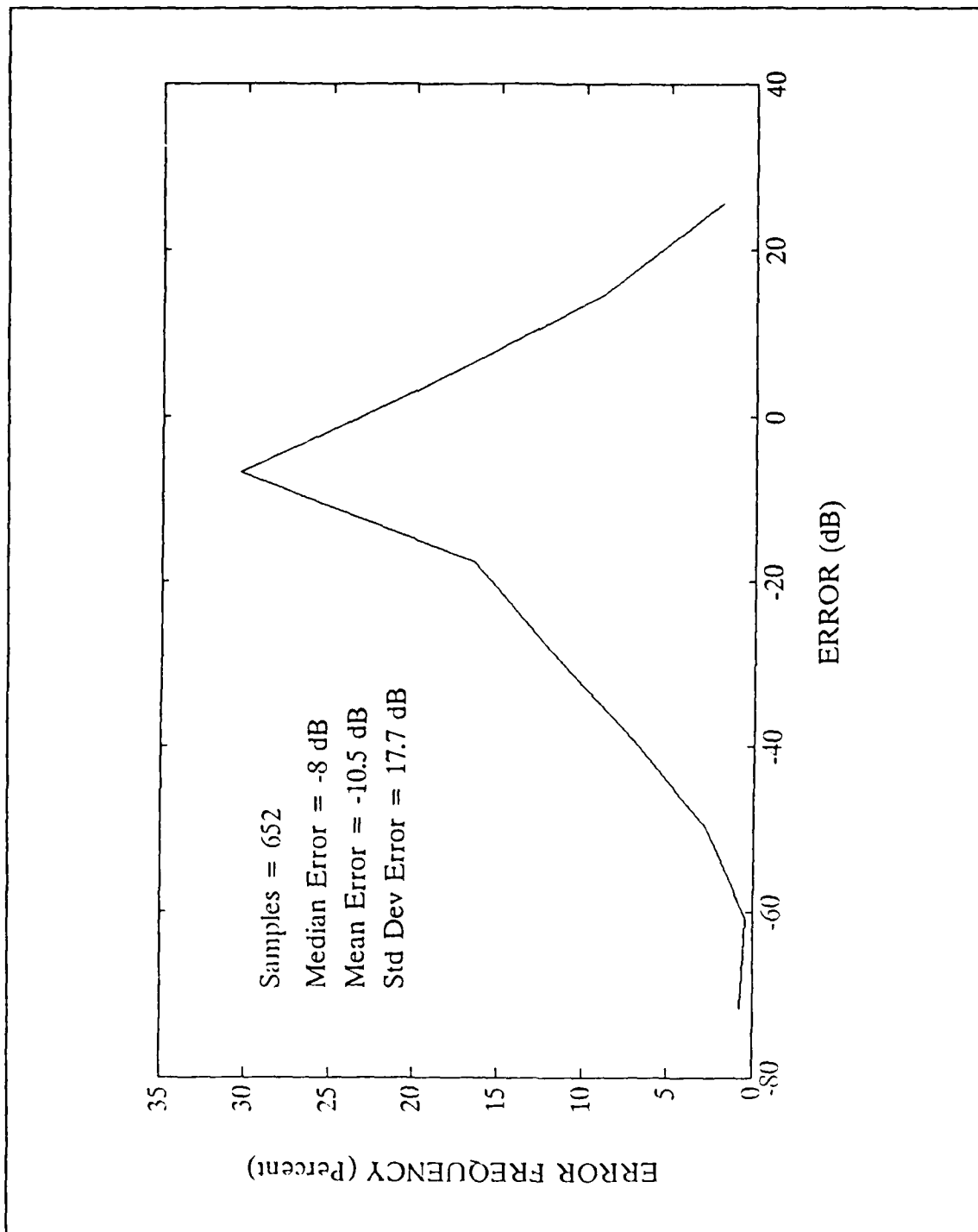
Figure 14. Frequency distribution of IONCAP-PC 2.5 prediction errors for long path lengths.

V. COMPARISON OF IONCAP-PC 2.5 WITH ADVANCED PROPHET

A. ASSUMPTIONS

The same CCIR data bank, used in Reference 3, was used to make a statistical analysis for prediction accuracy of IONCAP and PROPHET. For making a comparison of these two programs, 1,961 cases were run using Method 17 for IONCAP and the Field Strength option for PROPHET. The lines of the graphs contained in this chapter merely connect data points.

B. ANALYSIS

Medium and long path data for IONCAP-PC 2.5, that has already been analyzed in Figures 13 and 14, respectively, will be used for the comparison with PROPHET. The results of the analysis for IONCAP-PC 2.5, that are presented in Figure 15 will be used for the comparison with PROPHET, for short path data.

1. Short Path Data

The error frequency versus error for PROPHET for the short paths is shown in Figure 16. It is seen in Figures 15 and 16 that the median error of IONCAP is closer to zero than the error from PROPHET. The standard deviation error for IONCAP is much smaller than the error from PROPHET. Therefore, IONCAP is much more accurate than PROPHET for short path predictions. The same is concluded from Figure 17, which shows the cumulative distribution of the absolute value of prediction errors, for short paths, for both models. Note that 90% of IONCAP data is included between -20 dB and +20 dB error, however for PROPHET, only 65% of the data is included in this range.

2. Medium Path Data

In Figure 18, the error frequency versus the error is shown, for PROPHET, for medium paths. From Figures 13 and 18 it is difficult to conclude which of the models is more accurate, since their median error values and standard deviations are close. However, it can be seen from Figure 19 that 92% of IONCAP data is included between -20 and +20 dB error, while for PROPHET only 80% is included. Therefore, IONCAP is more accurate than PROPHET for medium paths.

3. Long Path Data

In Figure 20, the error frequency versus the error is shown, for PROPHET, for long paths. In Figure 21, the cumulative frequency versus error is shown for both pro-
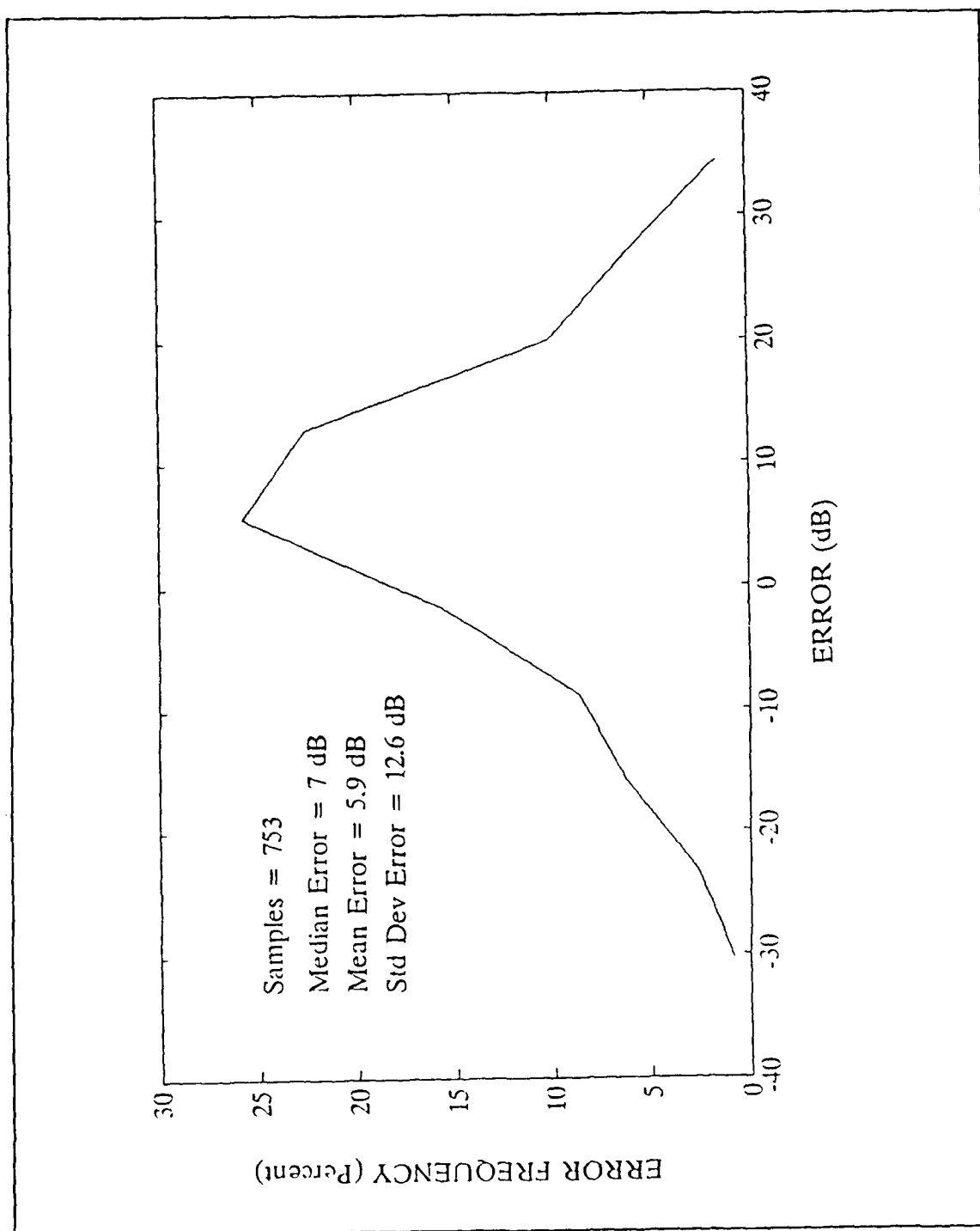
Figure 15. Frequency distribution of IONCAP-PC 2.5 prediction errors for short paths, for 753 samples.

Figure 16.   Frequency distribution of PROPHET prediction errors for short paths.

The chart shows ERROR FREQUENCY (Percent) on the vertical axis versus ERROR (dB) on the horizontal axis.

Samples = 753
Median Error = -14 dB
Mean Error = -17.4 dB
Std Dev Error = 20.9 dB

Figure 17.   Cumulative distribution of the absolute value of IONCAP and PROPHET prediction errors for short paths.
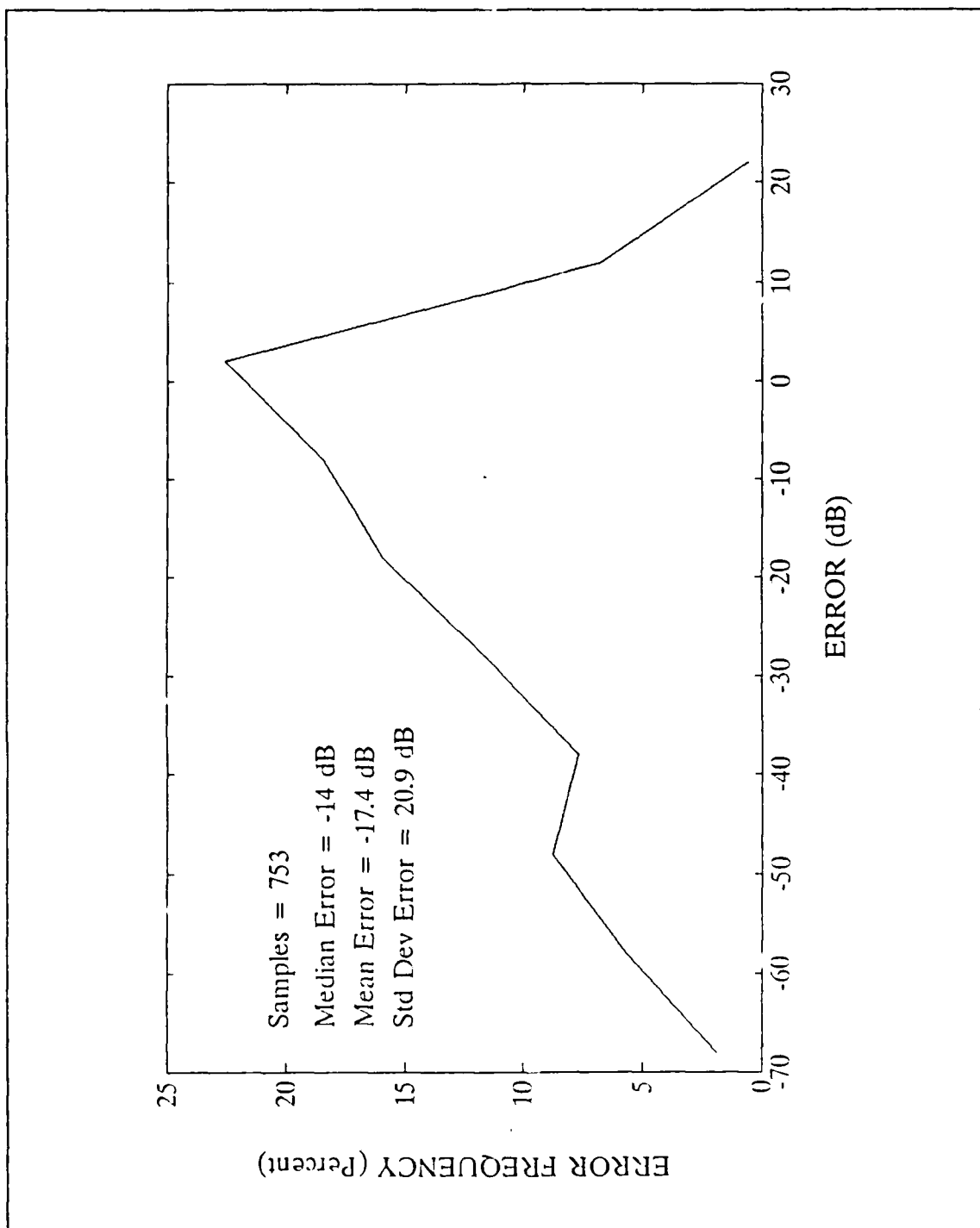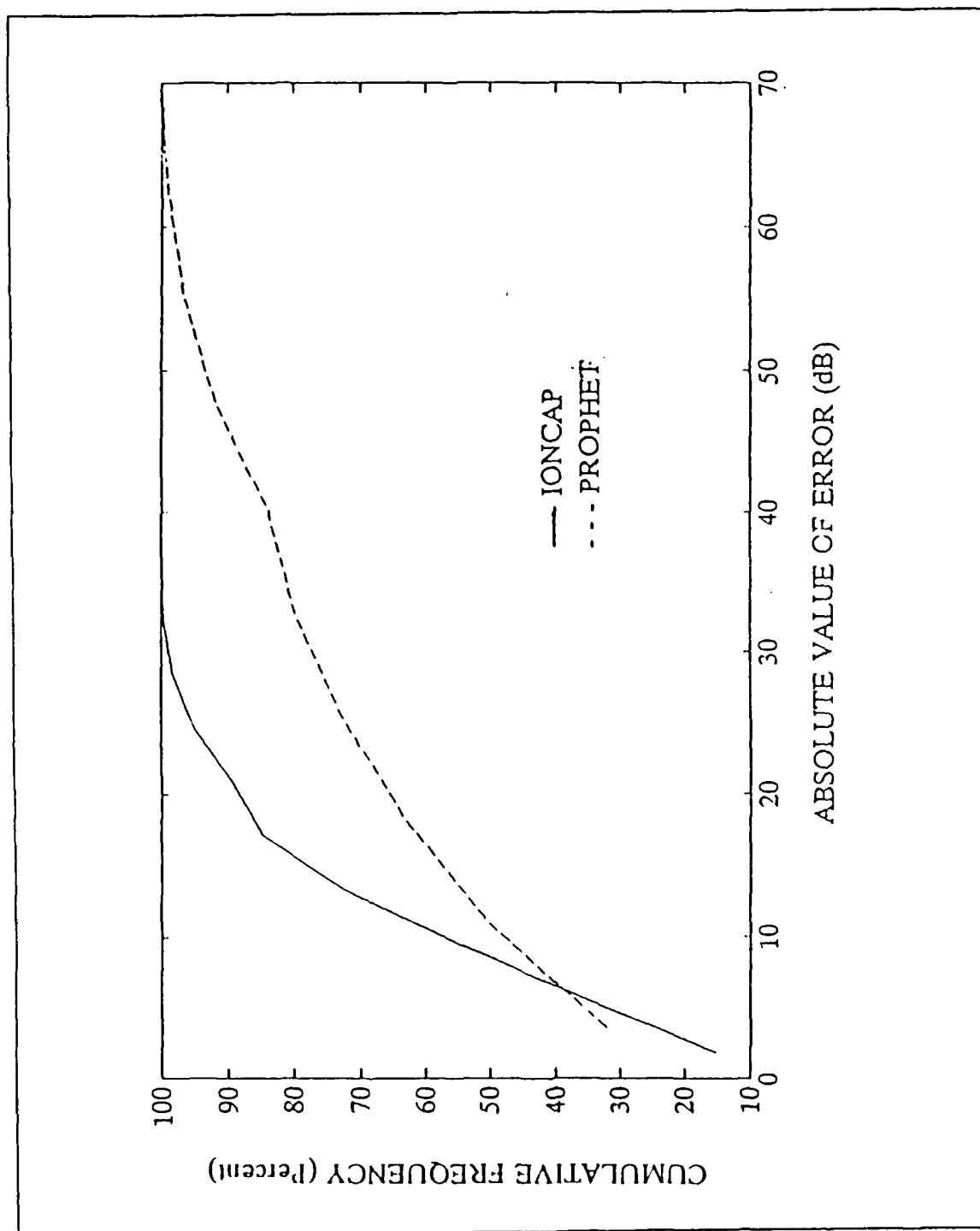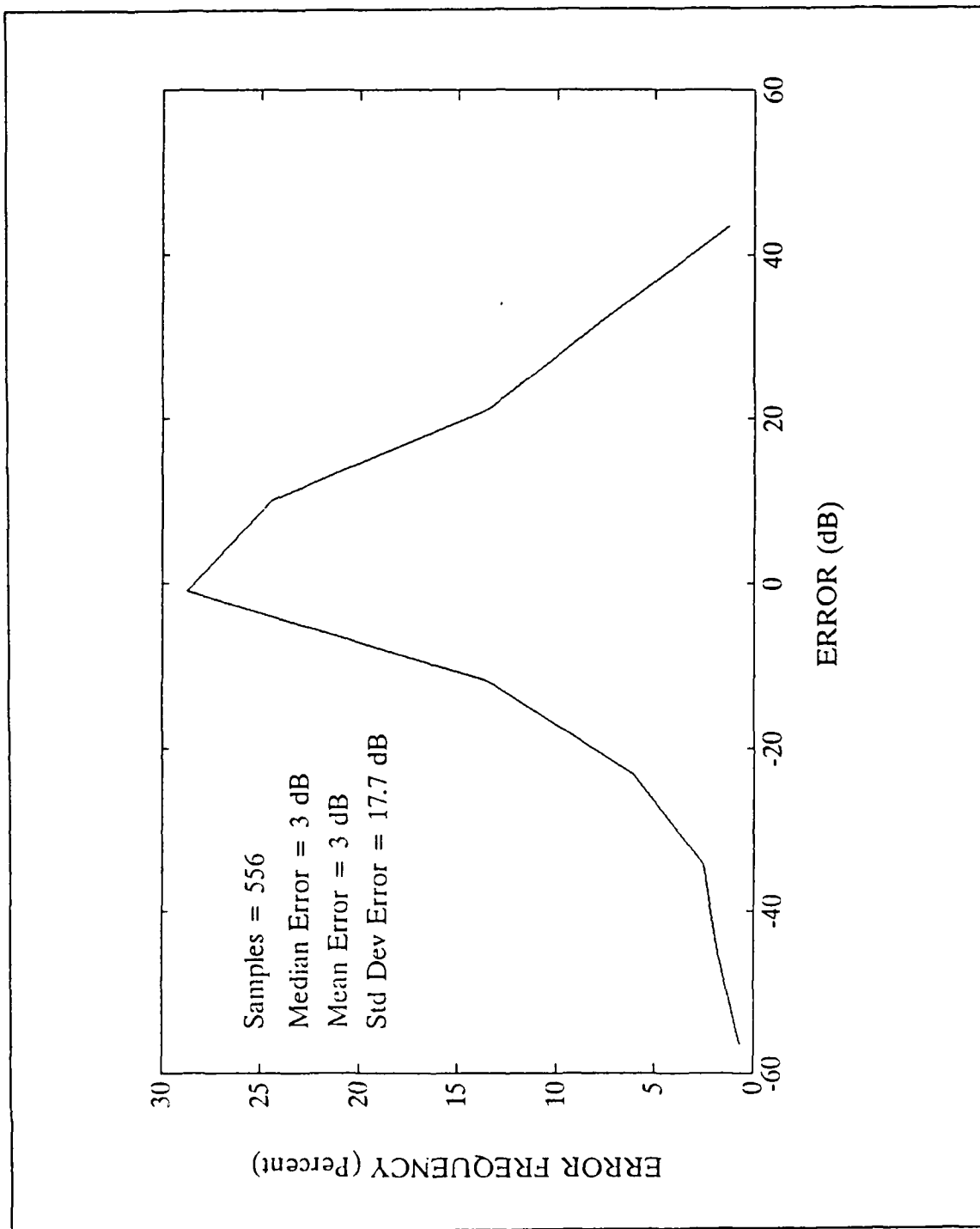
Figure 18. Frequency distribution of PROPHET prediction errors for medium paths.
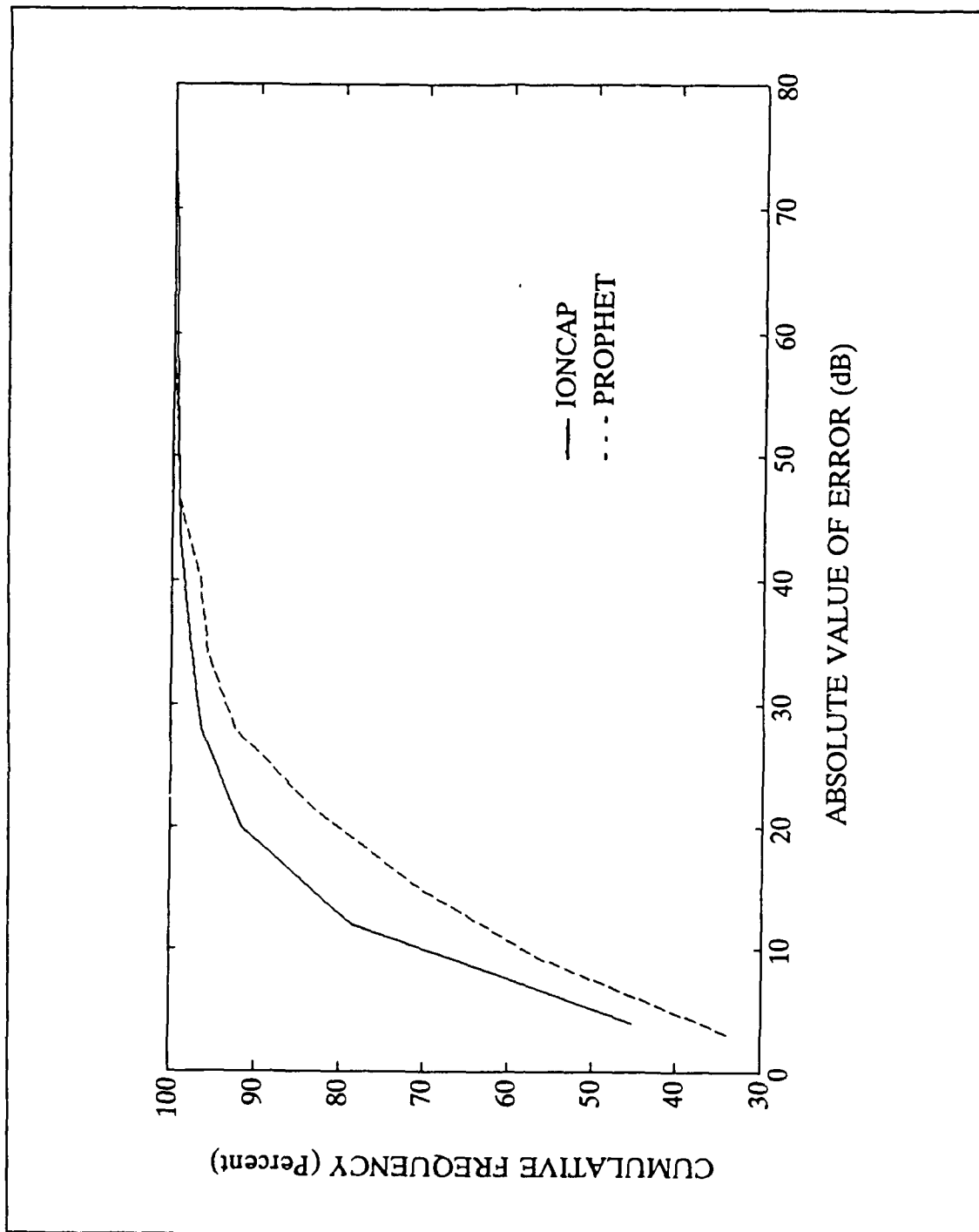
Figure 19.   Cumulative distribution of the absolute value of IONCAP and
PROPHET prediction errors for medium paths.

grams, for long paths. By comparing Figure 14 with Figure 20 it is seen that the median error is very close to zero for PROPHET (-1 dB), and relatively high for IONCAP (-8 dB). The standard deviation is a little higher for PROPHET (19.9 dB) than for IONCAP (17.7 dB). Therefore, it can be concluded that PROPHET is slightly more accurate than IONCAP for long path predictions. This is more obvious in Figure 21 where 82% of PROPHET data is included between -20 dB and +20 dB of error while only 78% of IONCAP data is included.

4. Macroscopic View of All Path Data

The prediction analysis for IONCAP and PROPHET for the data from all paths is presented in Figures 22 and 23 respectively. It can be seen that the two models have about the same median error. The standard deviation error is much higher for PROPHET. Therefore, IONCAP is more accurate than PROPHET. In Figure 24, the cumulative frequency versus the absolute error is shown for IONCAP and PROPHET for data from all paths. It can be seen that 81% of IONCAP data is included between -20 dB and +20 dB error and only 70% of PROPHET data is included. In general, it is concluded that IONCAP is more accurate than PROPHET.

5. Paths Comparison for PROPHET

In Figure 25, error frequency versus error is shown for short, medium and long paths, for PROPHET. This information was accumulated from Figures 16, 18 and 20. In Figure 26, cumulative frequency versus absolute error is shown, for these paths, for PROPHET.

It is seen in Figures 25 and 26 that PROPHET yields high errors during predictions of short path circuits.

By comparing the median error of PROPHET, for short, medium and long paths (Figures 16, 18, and 20), it is concluded that PROPHET field strength predictions are consistently low on short and long paths, as could be expected for a conservative program.

6. Polar Paths

For this study, a path is defined as polar if:

a. one or both stations of a circuit are located above 60° latitude, or

b. any part of the path between stations crosses the zone between the 60° and 90° latitude.

Almost all of the polar paths of this CCIR data bank have both stations below 60° latitude, and a portion of the path crosses the zone between the 60° and 90° latitude. Unfortunately, there is not any path in the CCIR data bank that crosses the Auroral

Figure 20.   Frequency distribution of PROPHET prediction errors for long paths.

Figure 21.   Cumulative distribution of the absolute value of IONCAP and PROPHET prediction errors for long paths.
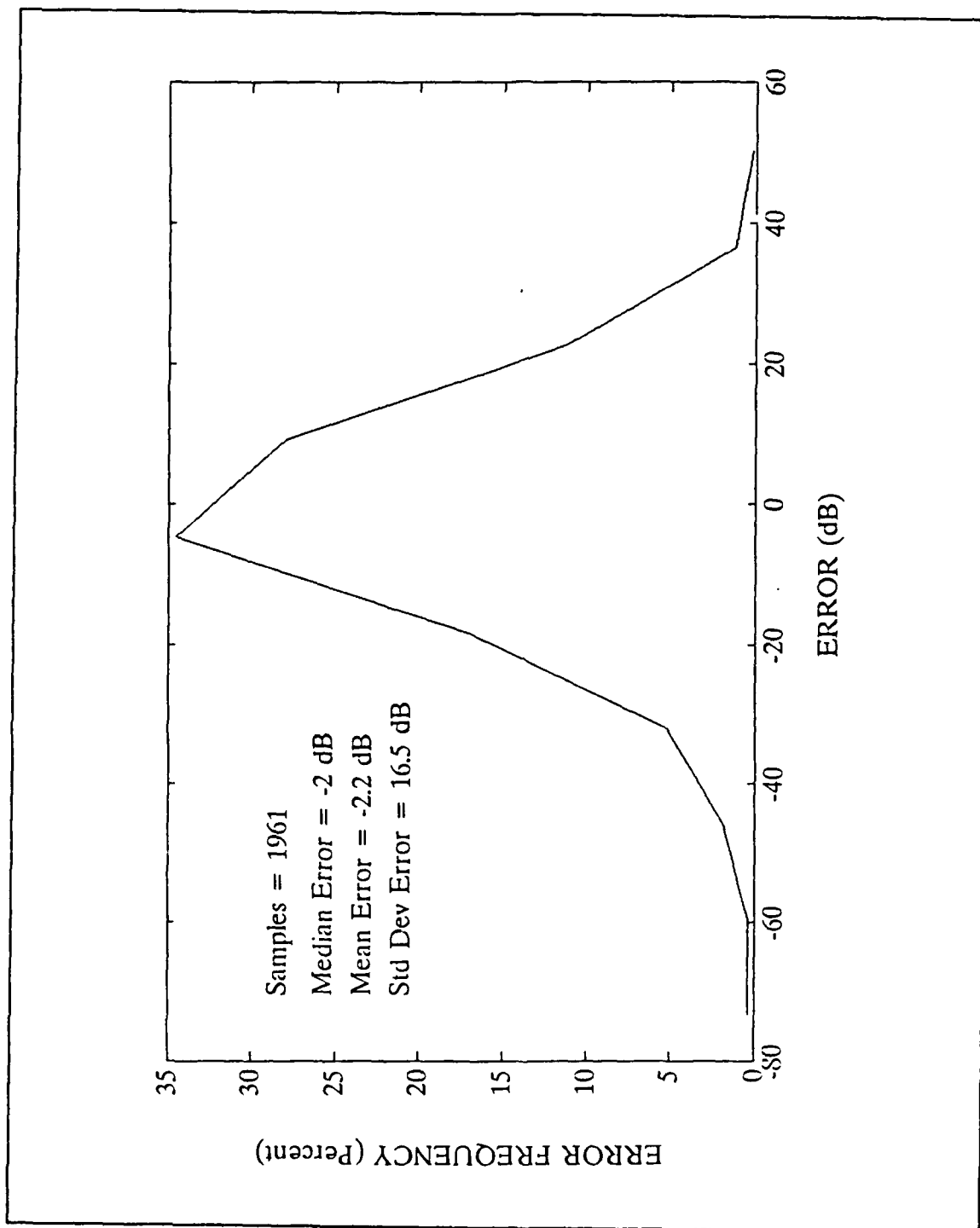
Figure 22. Frequency distribution of IONCAP prediction errors.

The chart shows:
- ERROR FREQUENCY (Percent) on the vertical axis, ranging from 0 to 35
- ERROR (dB) on the horizontal axis, ranging from -80 to 60

Text within the chart:
Samples = 1961
Median Error = -2 dB
Mean Error = -2.2 dB
Std Dev Error = 16.5 dB

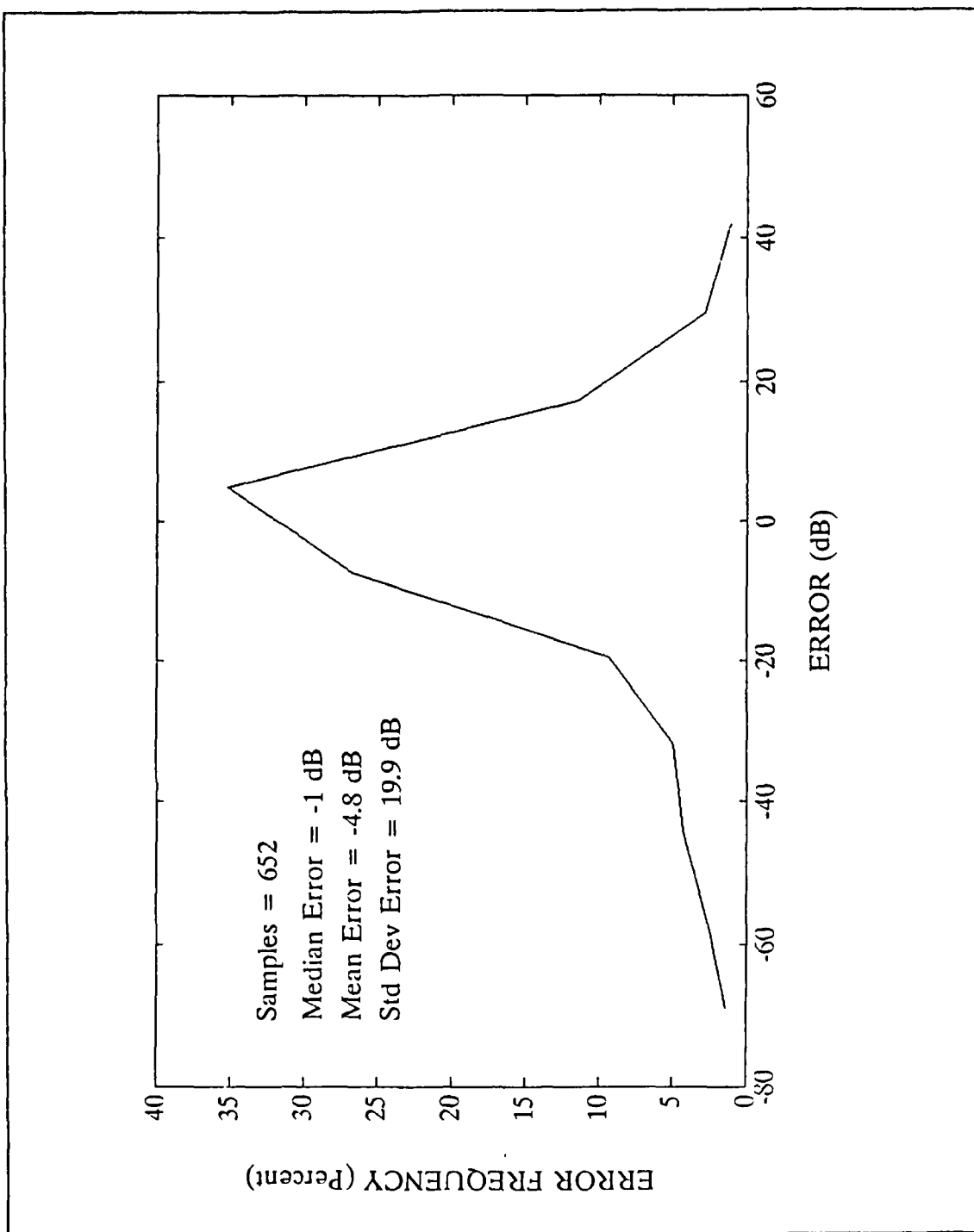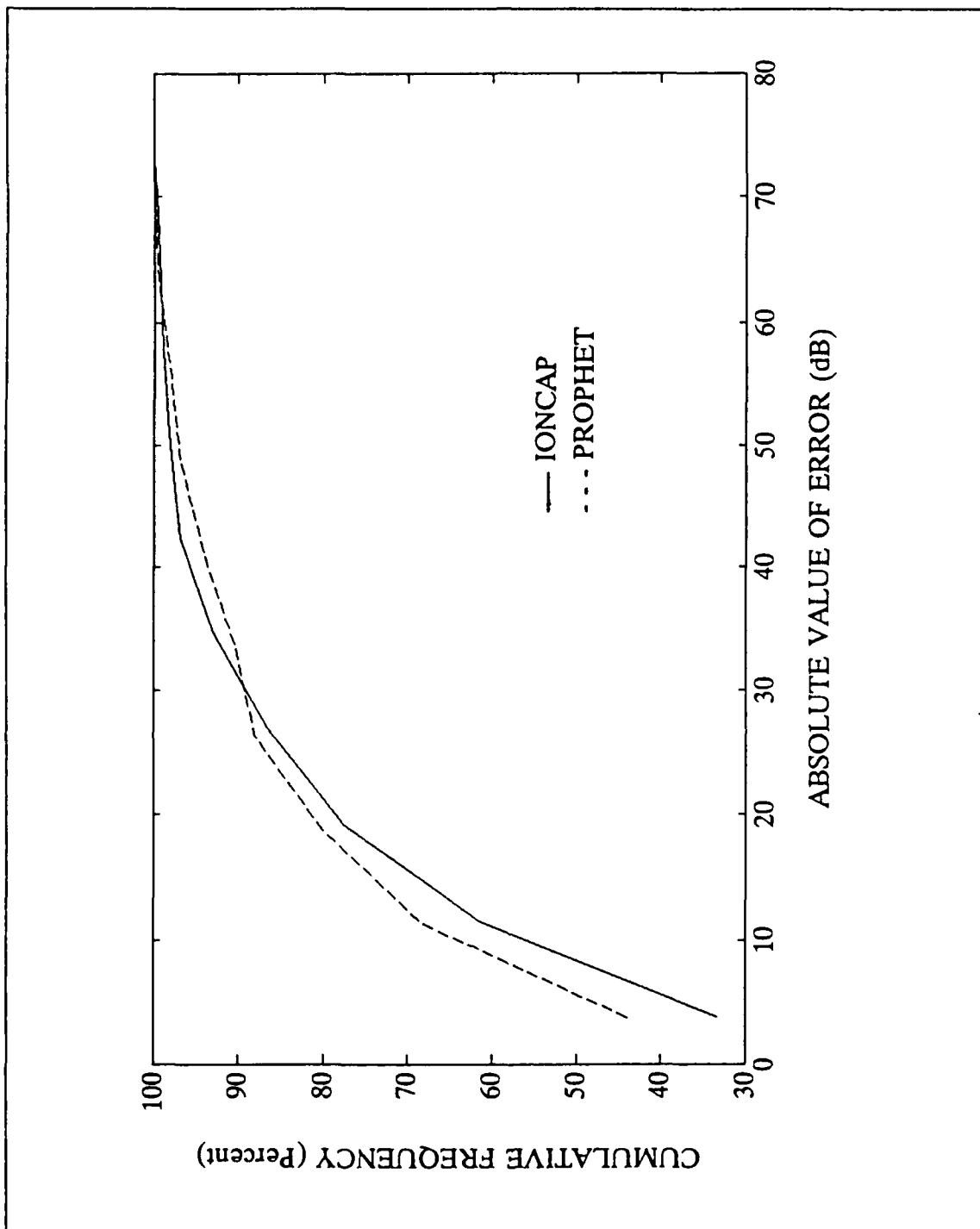**Figure 23.** Frequency distribution of PROPHET prediction errors.

39

Figure 24. Cumulative distribution of the absolute value of IONCAP and PROPHET prediction errors.

Figure 25. Frequency distribution of PROPHET prediction errors, for short, medium and long paths.

Figure 26. Cumulative distribution of the absolute value of PROPHET prediction errors, for short, medium and long paths.

zones, where severe ionospheric disturbance occurs. The "polar" paths that are analyzed below are all classified as long paths and their stations are below 60° latitude.

The frequency distribution of IONCAP and PROPHET prediction errors is shown in Figures 27 and 28 respectively, for polar paths. It is known that most ionospheric models are less accurate for predictions of polar paths than for other paths. For PROPHET, this can be observed, since the standard deviation for the polar paths is the highest of those already seen (23.4 dB). However, this is not true for IONCAP, since the median error of polar paths (-5 dB) is closer to zero than the median error of long paths (-8 dB) which already contain polar paths. The standard deviation of polar paths (15.3 dB) is also less than the standard deviation of long paths (17.7 dB). Therefore, IONCAP is better at predicting the field strength of polar paths, as previously defined, than predicting long paths, as supported by Figures 14 and 27. Figures 11 and 29 also demonstrate that, for IONCAP, between -20 and +20 dB error, 86% of the data of polar paths is contained. On the other hand, only 76% of the data of long paths is contained. This also supports the fact that the paths, defined as polar, are not actually auroral region polar paths.

In Figure 29, the cumulative distribution of the absolute value of the prediction error is shown, for IONCAP and PROPHET, respectively. It can be seen that 86% of IONCAP data is included between -20 and +20 dB error while only 73% of PROPHET data is included. Therefore, IONCAP is more accurate than PROPHET for "polar" path predictions.
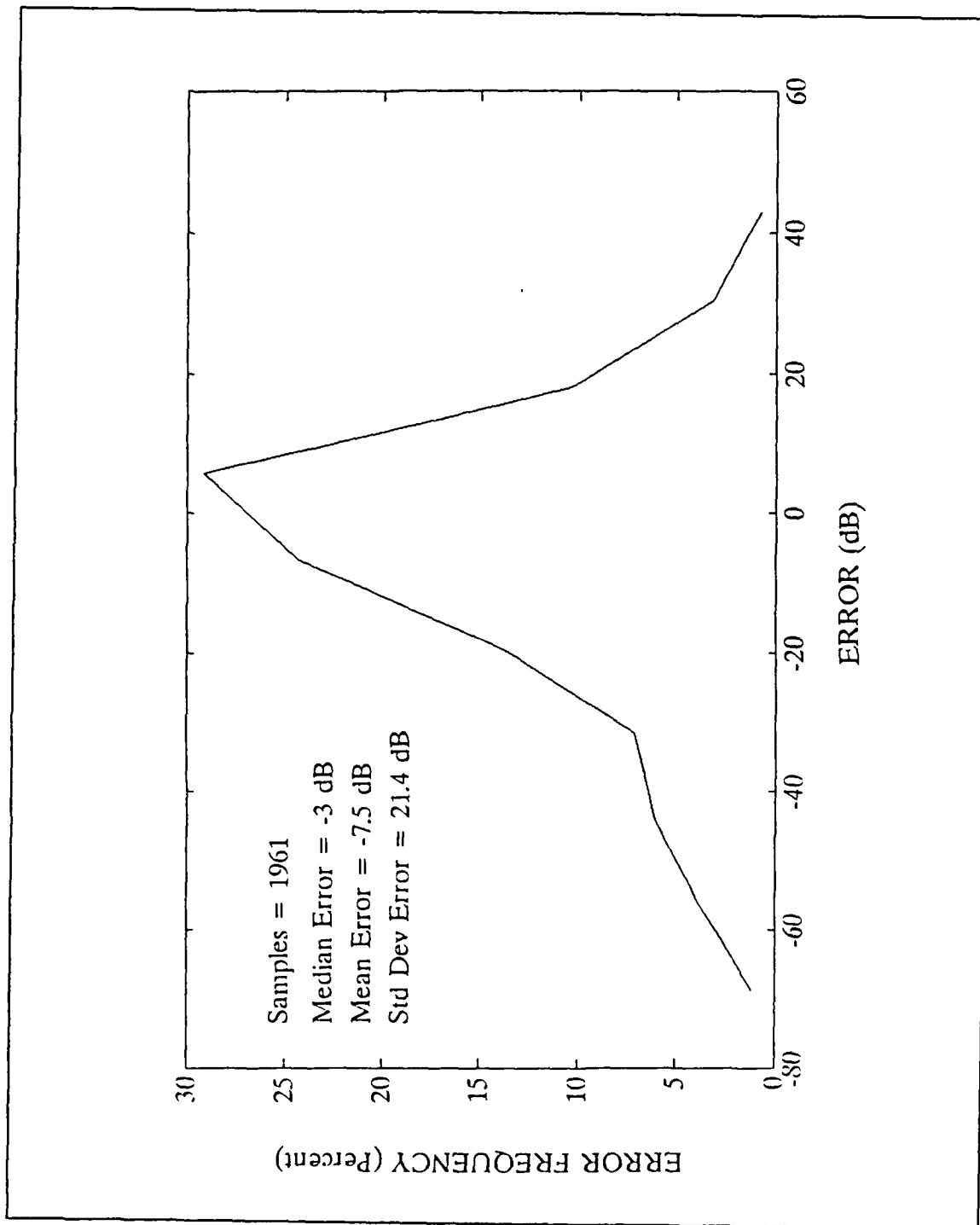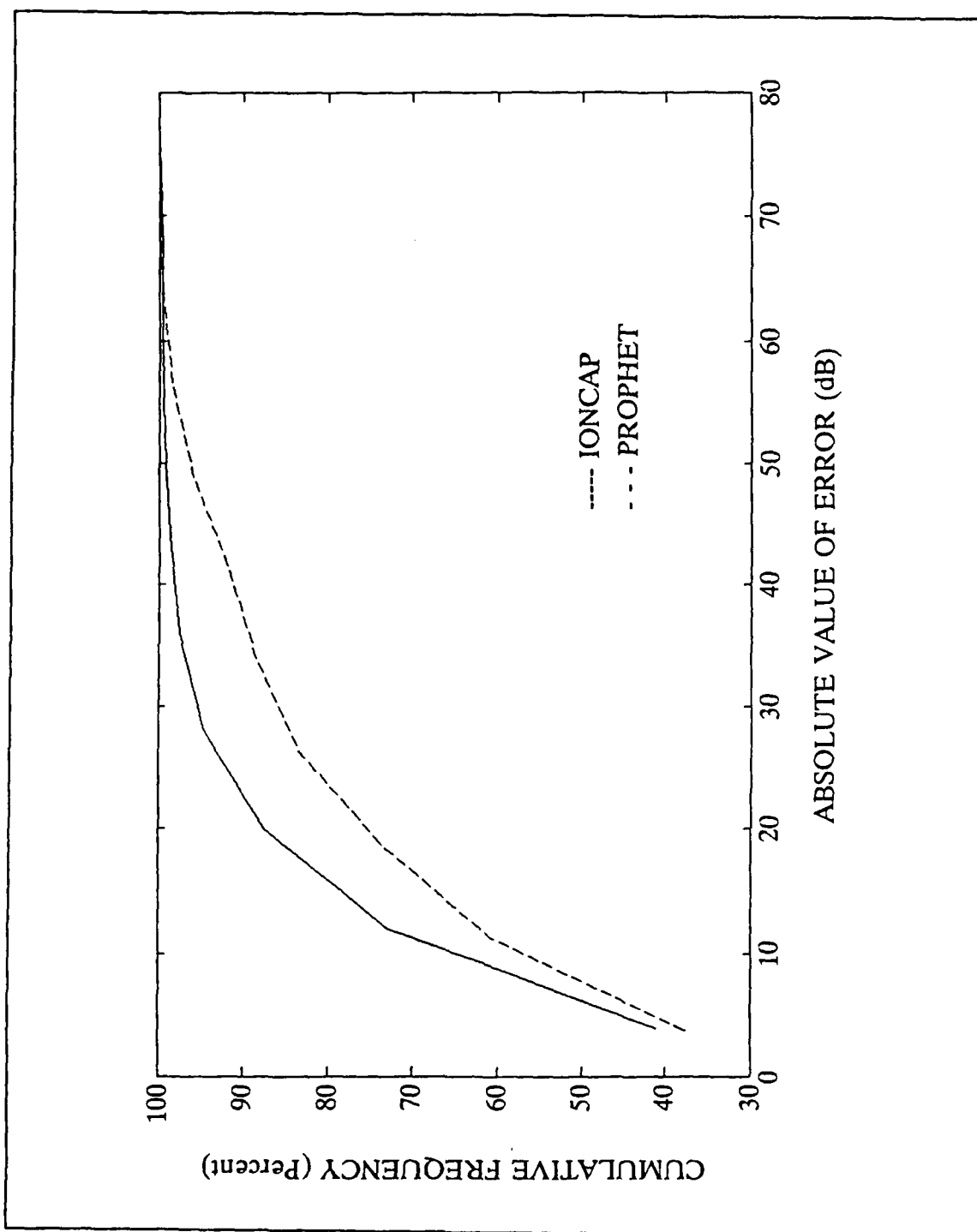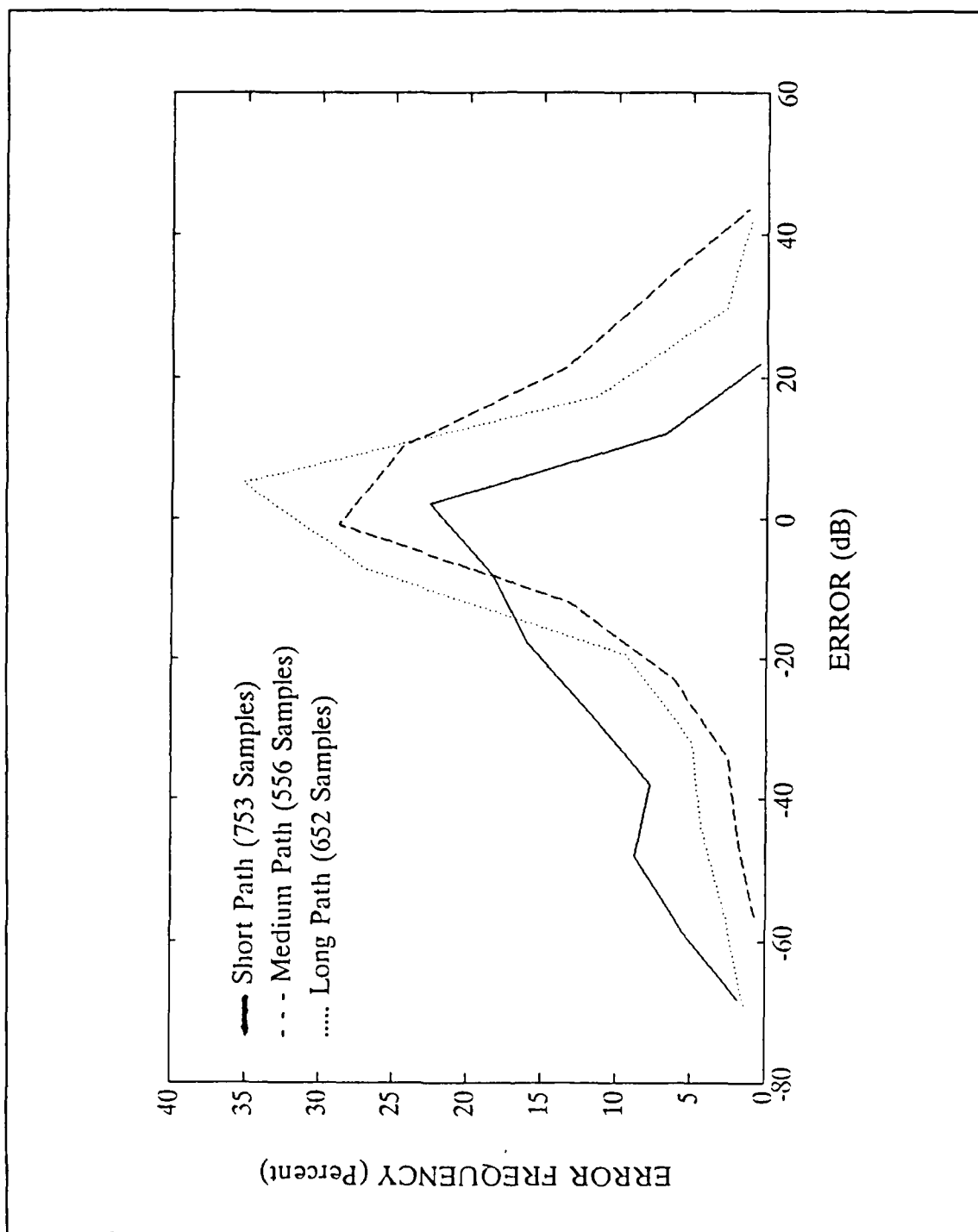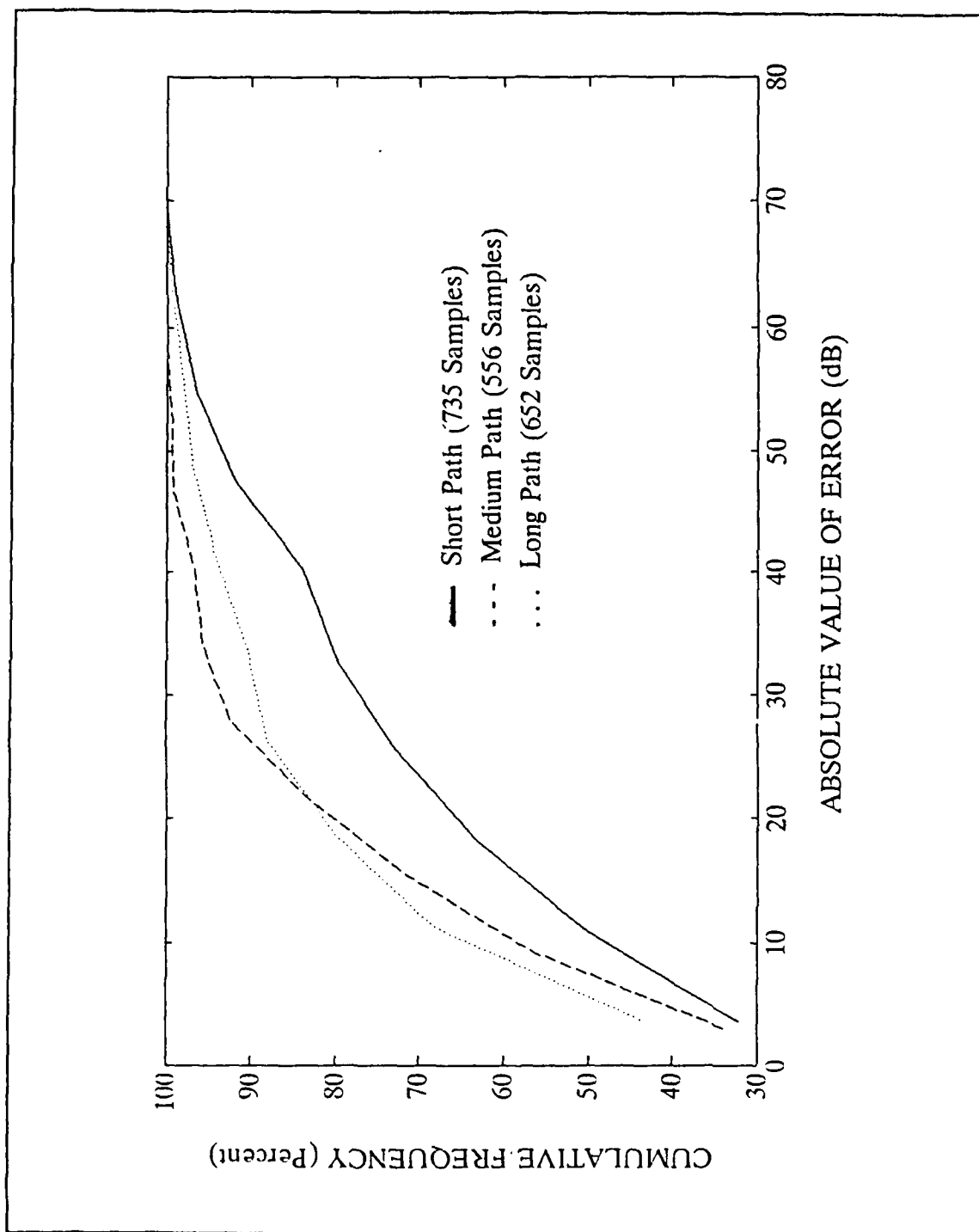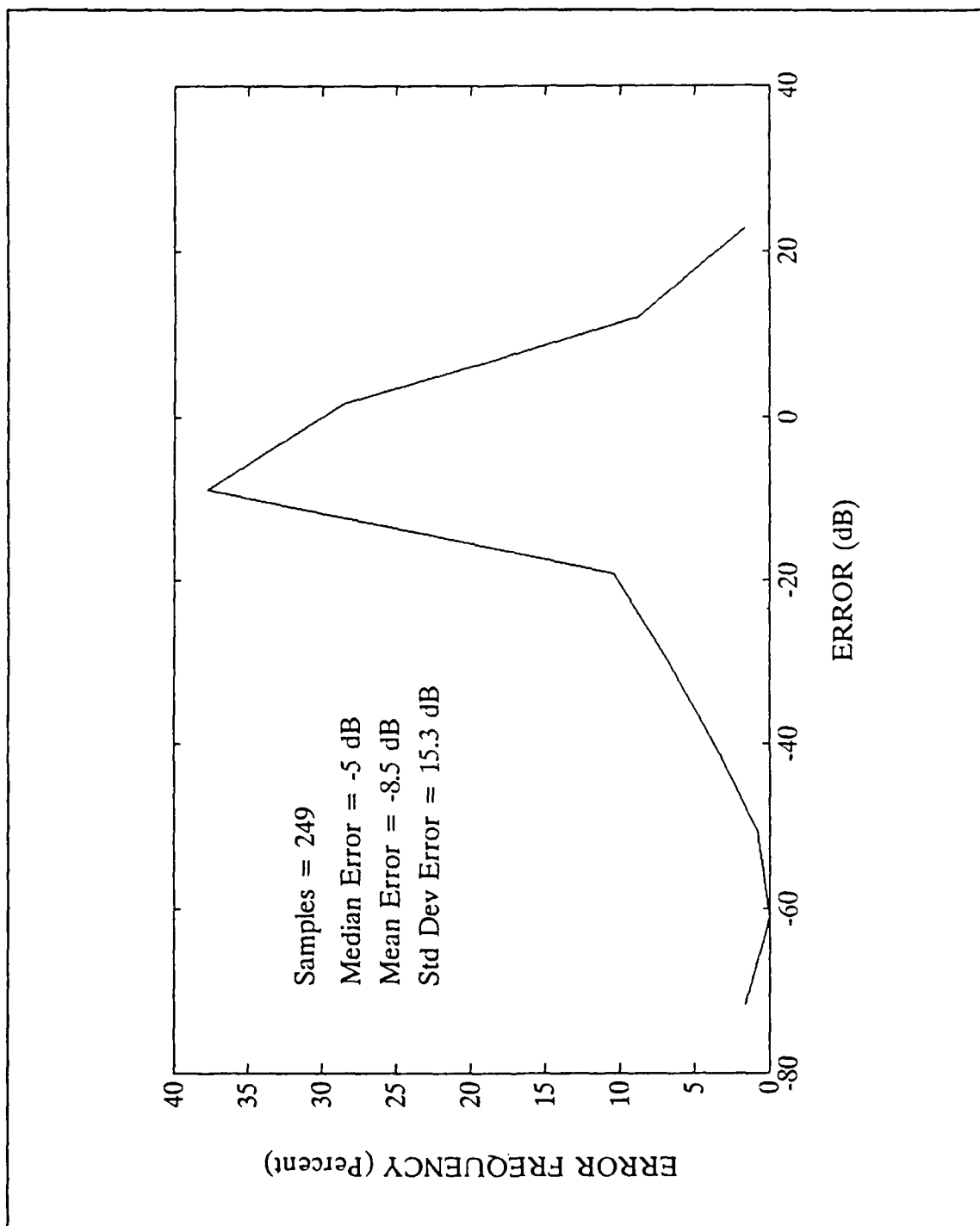
Figure 27.   Frequency distribution of IONCAP prediction errors for polar paths.
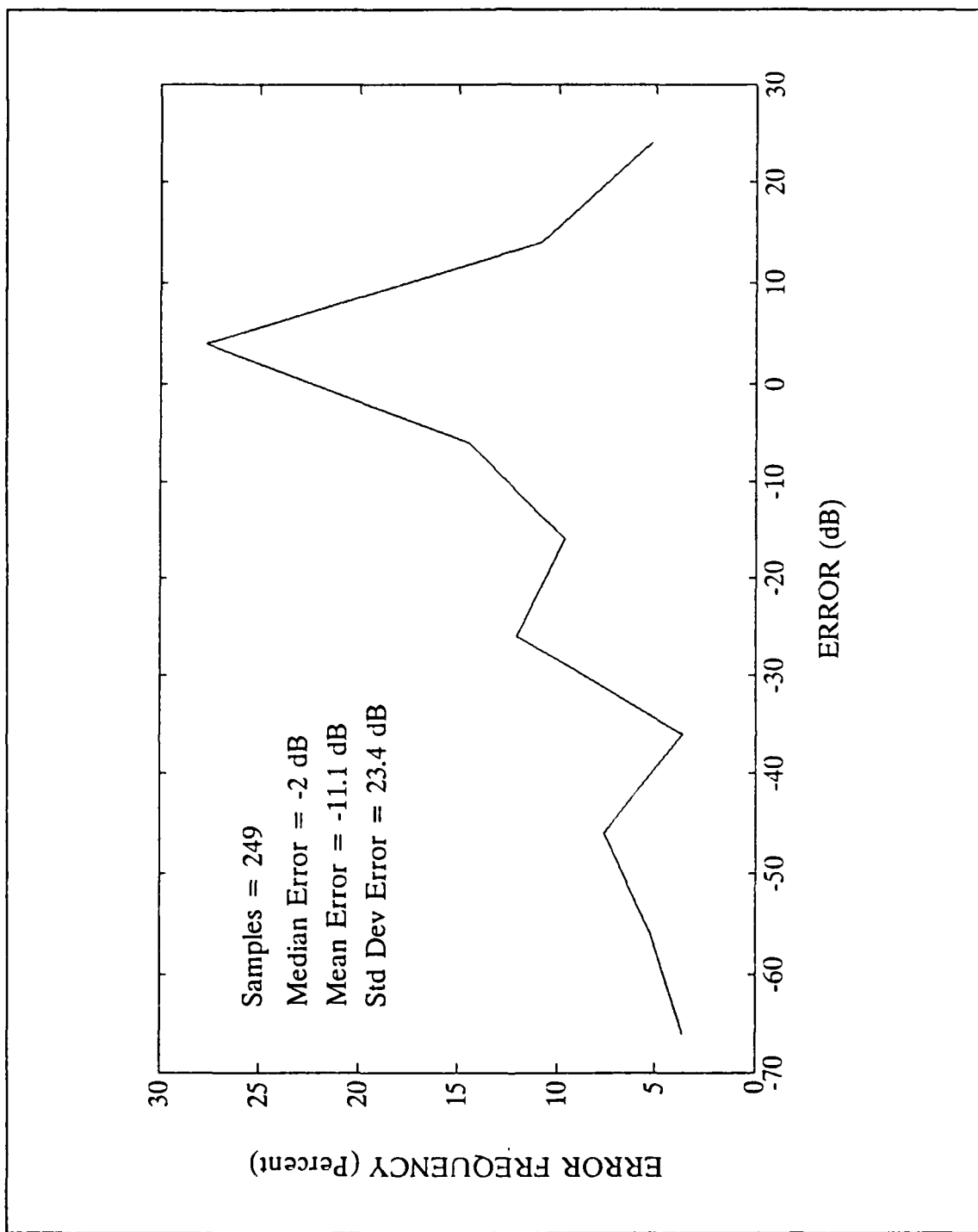
Figure 28. Frequency distribution of PROPHET prediction errors for polar paths.

The graph displays:
- Samples = 249
- Median Error = -2 dB
- Mean Error = -11.1 dB
- Std Dev Error = 23.4 dB

X-axis: ERROR (dB), ranging from -70 to 30
Y-axis: ERROR FREQUENCY (Percent), ranging from 0 to 30

Figure 29.   Cumulative distribution of the absolute value of IONCAP and
PROPHET prediction errors, for polar paths.

VI. CONCLUSIONS AND RECOMMENDATIONS

The conclusions that were extracted from the last two chapters are summarized below when comparing to the CCIR field strength data base:

- IONCAP 85.04 predictions are most accurate for short, and medium paths [Ref. 3].

- IONCAP-PC 2.5 predictions are most accurate for medium paths.

- The random component of the prediction error for IONCAP 85.04 increases with increasing path length [Ref. 3]. This is not true for the prediction error of IONCAP-PC 2.5.

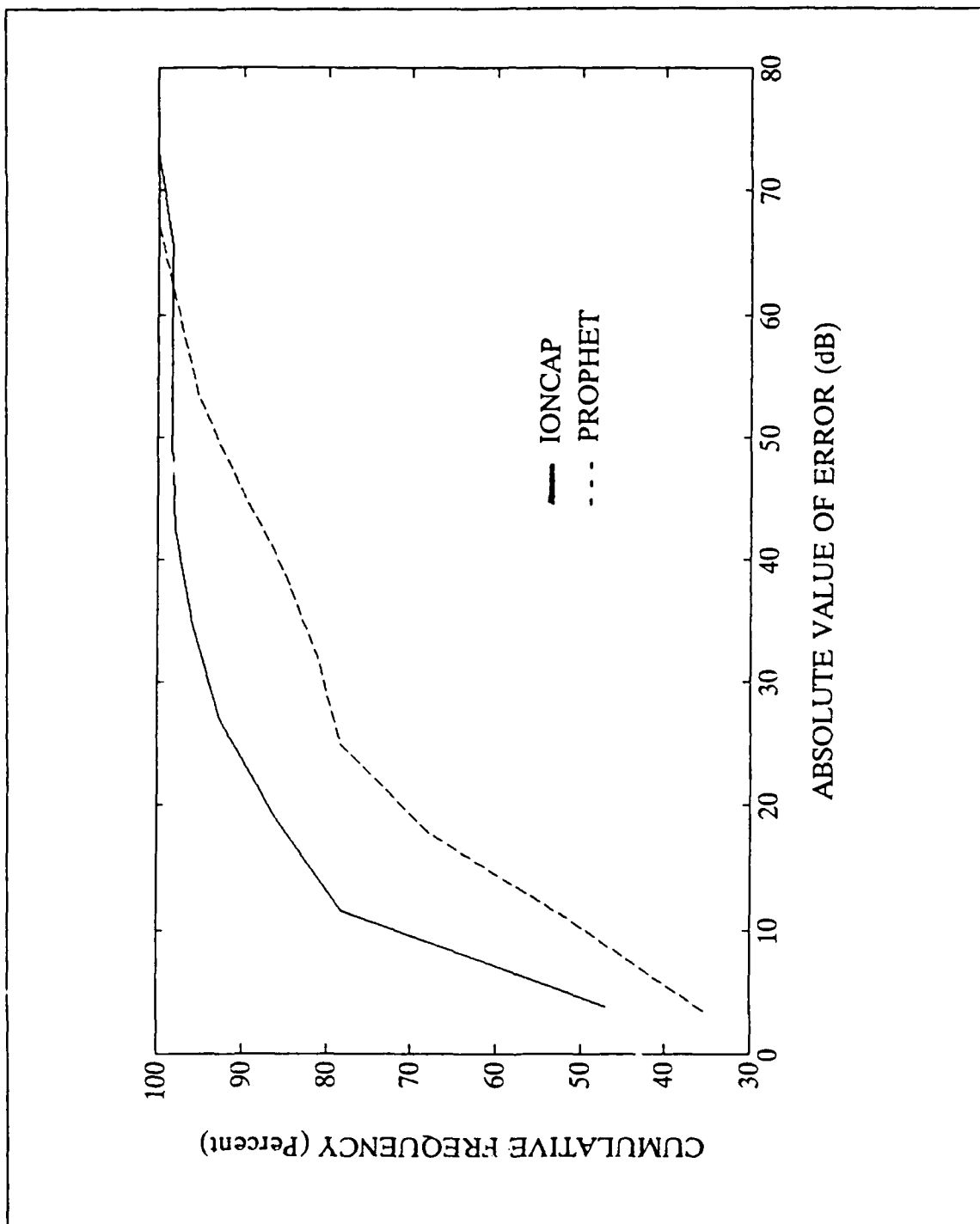- IONCAP 85.04 [Ref. 3] and IONCAP-PC 2.5 field strength predictions are consistently low on medium and long paths.

- IONCAP-PC 2.5 field strength predictions are, in general, slightly more accurate than IONCAP 85.04 field strength predictions.

- In IONCAP-PC 2.5, a great improvement is observed in predicting long path circuits in comparison with IONCAP 85.04. The improvement for predictions of medium paths circuits is small, and there is no improvement for predictions of short path circuits.

- The random component of the prediction error for PROPHET increases with decreasing path length, since PROPHET is less accurate for predictions of field strength of short path circuits than IONCAP.

- IONCAP is generally more accurate than PROPHET.

- PROPHET field strength predictions are consistently low on short and long paths.

- IONCAP is more accurate than PROPHET for "polar" path field strength predictions.

In the future, a further analysis of MINIPROP should be conducted. A model called AMBCOM has become available at NPS [Ref. 10]. The special features of this code are a model of the electron density profile in the high latitude ionosphere (including the auroral zone) and a model for computing the auroral absorption. PROPHET 4.0 is available and a new version of IONCAP-PC for polar regions (ICECAP) will also be available soon. An evaluation of these models must also be conducted.

An area of great interest concerning ionospheric propagation, is the area near the poles. Professor Tudor Jones from the University of Leichester in England has collected data for measured electric field strength for true polar paths [Ref 11]. An analysis should be conducted by using this data bank for all models.

47

APPENDIX   MINIPROP RESULTS

MINIPROP 3.0 is a PC-based computer program for predicting ionospheric propagation which covers the HF band (3-30 MHz). It predicts received signal levels using an algorithm that searches the potential ionospheric modes to find the mode that provides the strongest received signal level [Ref. 12].

IONCAP and PROPHET outputs are electric field strength predictions in dB above 1 μV/m, while the primary MINIPROP output is a voltage prediction at the input of the receiver in dB above 0.5 μV. Therefore, MINIPROP output must be transformed to field strength values in order to be compared with the measured values of the CCIR data bank by using the formulas:

$$P_a = \frac{E^2}{120\pi}$$

where

P$_a$ is the power flux at the antenna in Watts m^{-2},

E is the electric field strength in Volts/m; and

$$P = \frac{V^2}{R} = P_a \times A_e$$

where

P is the received power at the input of the receiver in Watts,

V is the voltage at the input of the receiver in Volts,

R is the receiver input resistance in Ωhms (R = 50Ω),

A$_e$ is the effective aperture of the antenna in m^2.

For a halfwave dipole antenna the effective aperture A$_e$ is given by

$$A_e = \frac{\lambda^2}{4\pi} \times 1.64$$

where λ is the wavelength in meters.

By using the formulas mentioned above, the electric field strength E is given by

$$E = V + 20 \log f - 32$$

where

E is the electric field strength in dB above 1 μV/m,

V is the voltage at the input of the receiver in dB above 0.5 μV and

f is the frequency in MHz.

In order to evaluate the performance of MINIPROP, 122 cases were run with IONCAP, PROPHET and MINIPROP. All these cases were for long paths.

In Figure 30, the frequency distribution of the prediction errors for MINIPROP is shown. In Figure 31, the cumulative distribution of the prediction errors for the three models is shown. From Figure 30 it is seen that the median error for MINIPROP is 14 dB. For the same data, the median errors for IONCAP and PROPHET are -9 dB and -10 dB, respectively. The standard deviation error for MINIPROP is 15.2 dB; for IONCAP and PROPHET 15 dB and 20 dB, respectively. It is concluded that while IONCAP and PROPHET give conservative predictions, MINIPROP gives optimistic predictions. From Figure 31, it is concluded that MINIPROP has about the same performance as PROPHET and is less accurate than IONCAP for the cases analyzed.

However, since only one category of paths was analyzed and the number of the samples was limited, a further study for the performance of MINIPROP is needed.

Samples = 122
Median Error = 14 dB
Std Dev Error = 15.2 dB
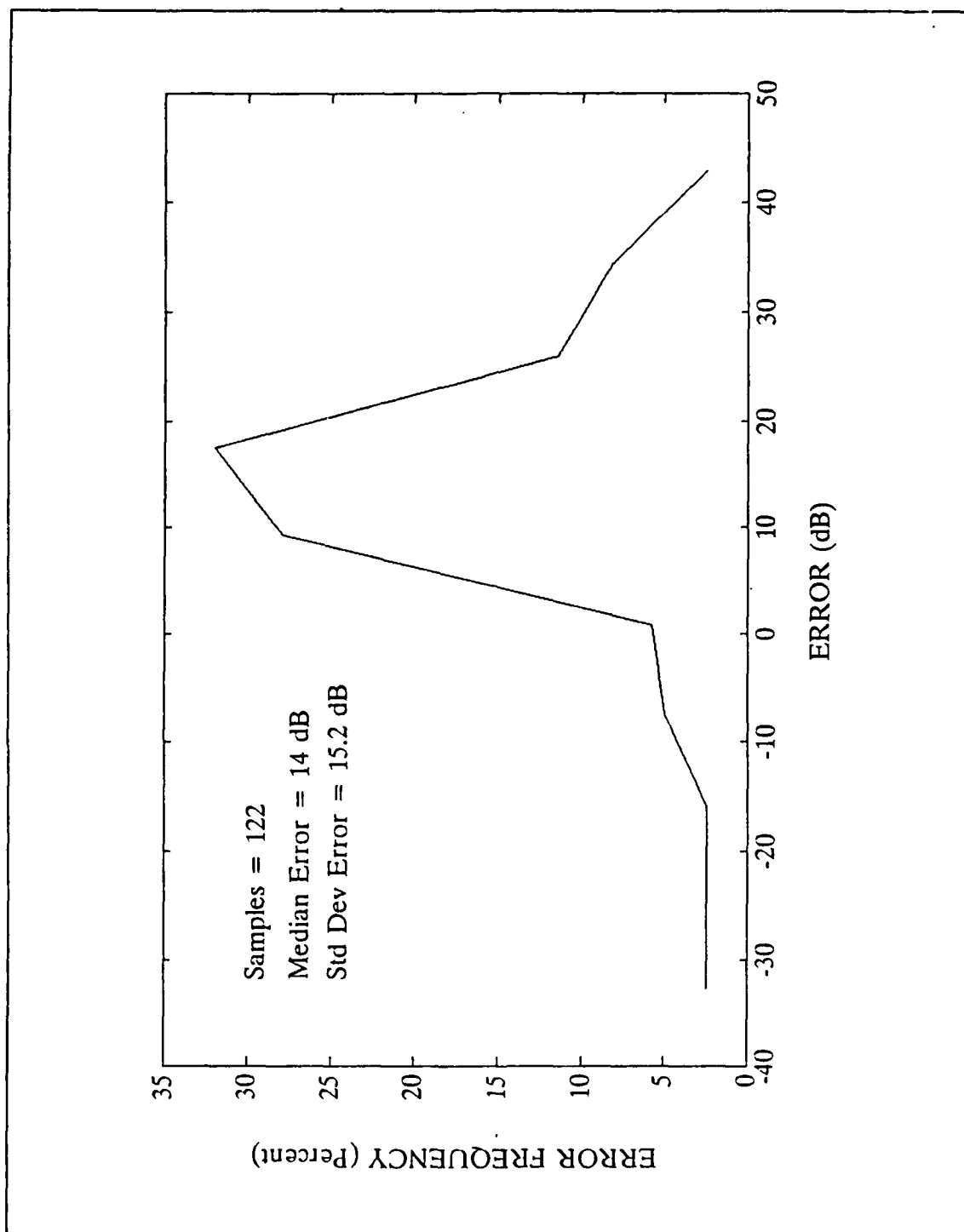
ERROR FREQUENCY (Percent)

ERROR (dB)

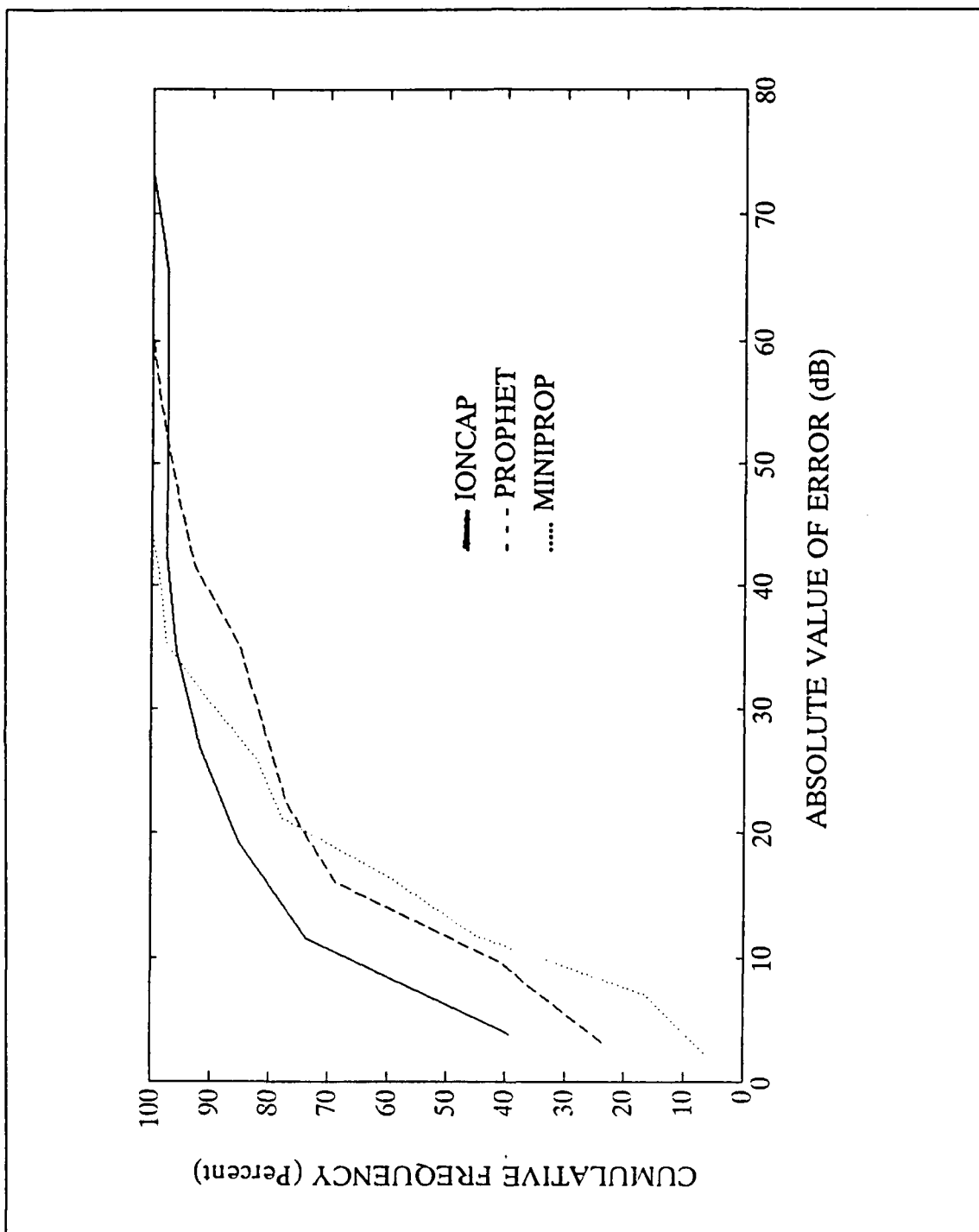Figure 30.   Frequency distribution of MINIPROP prediction errors.

Figure 31. Cumulative distribution of the absolute value of IONCAP, PROPHET and MINIPROP prediction errors.

LIST OF REFERENCES

1. *Ionospheric Radio Propagation,* NBS Circular 462, Central Radio Propagation Laboratory, 1948.

2. Kenneth Davies, *Ionospheric Radio Propagation,* National Bureau of Standards, 1965.

3. A. A. Tomko, "Statistical Analysis of the Prediction Accuracy of HF Propagation Models", presented at the National Radio Science Meeting, Boulder, Colorado, January 1989.

4. Mark Daehler, *NRL VOA Modifications of IONCAP as of 12 July 1988,* Memorandum Report 6514, Naval Research Laboratory, Washington DC, 1989.

5. Nicholas M. Maslin, *HF Communications: A Systems Approach,* Plenum Press, New York, 1987.

6. Gerhard Braun, *Planning and Engineering of Shortwave Links,* Siemens, Berlin, 1986.

7. L. R. Teters, J. L. Lloyd, G. W. Haydon, D. L. Lucas, *Estimating the Performance of Telecommunication Systems Using the Ionospheric Transmission Channel,* Volume 2 (draft), Institute for Telecommunication Sciences, September 1978.

8. R. B. Rose, *Advanced Prophet HF Assessement System,* Technical Document 692, Naval Ocean Systems Center, San Diego, April 1984.

9. D. B. Sailors, R. A. Sprague, W. H. Rix, *MINIMUF-85: An improved HF MUF Prediction Algorithm,* Technical Report 1121, Naval Ocean Systems Center, San Diego, July 1986.

10. Georgellen Smith, V. Elaine Hatfield, *AMBCOM User's Guide for Engineers,* SRI International, Menlo Park, California, 1987.

11. Private telephone conversation between Professor Richard W. Adler and Professor Tudor Jones, 4 May 1990.

12. Sheldon C. Shallon, *MINIPROP version 3 with mode searching,* W6EL Software, Los Angeles, 1988.

BIBLIOGRAPHY

1. D. B. Sailors, *Operators Manual for the United States Coast Guard, Advanced PROPHET System*, Naval Ocean Systems Center, San Diego, 1987.

INITIAL DISTRIBUTION LIST

No. Copies

1. Defense Technical Information Center   2
   Cameron Station
   Alexandria, VA 22304-6145

2. Library, Code 0142   2
   Naval Postgraduate School
   Monterey, CA 93943-5002

3. Chairman, Code EC   1
   Department of Electrical and Computer Engineering
   Naval Postgraduate School
   Monterey, CA 93943

4. Professor R. W. Adler, Code EC/Ab   5
   Department of Electrical and Computer Engineering
   Naval Postgraduate School
   Monterey, CA 93943

5. Professor W. R. Vincent, Code EC/Ja   1
   Department of Electrical and Computer Engineering
   Naval Postgraduate School
   Monterey, CA 93943

6. Professor S. Jauregui, Code EC/Ja   1
   Department of Electrical Engineering
   Naval Postgraduate School
   Monterey, CA 93943

7. Dr. Al Tomko   1
   The Johns Hopkins University
   Applied Physics Laboratory
   Johns Hopkins Road
   Laurel, MD 20707

8. Professor James Breakall   1
   CCSL/EE EAST
   Pennsylvania State University
   University Park, PA 16802

9. Mr. Bob Rose   1
   Naval Ocean Systems Center
   Code 722
   San Diego, CA 92152

10. Professor Robert Hunsucker　　　　　　　　　　　　　1
    1618 Scenic Loop
    Fairbanks, AK 99709

11. Mr. Dennis Sheppard　　　　　　　　　　　　　　　1
    Naval Security Group Support Activity
    Code GX
    3801 Nebraska Ave NW
    Washington, DC 20390-0008

12. George Hagn　　　　　　　　　　　　　　　　　　1
    SRI International
    1611 Kent St
    Arlington, VA 22209

13. USAISEC　　　　　　　　　　　　　　　　　　　1
    ATTN: ASB-SET-P (J. Mc Donald)
    Ft Huachuca, AZ 85613-5300

14. William Hickey　　　　　　　　　　　　　　　　　1
    Ball Aerospace Corporation (TT4)
    P.O. Box 1062
    Boulder, CO 80306

15. Wayne Bratt　　　　　　　　　　　　　　　　　　1
    Naval Ocean Systems Center
    Code 722
    San Diego, CA 92152

16. Lieutenant Steve Carder　　　　　　　　　　　　　1
    Naval Security Group Support Activity
    Code GX
    3801 Nebraska Ave NW
    Washington, DC 20390-0008

17. Embassy of Greece　　　　　　　　　　　　　　　2
    Naval Attache
    2228 Massachusetts Av., N.W.
    Washington D.C. 20008

18. Lieutenant George Giakoumakis　　　　　　　　　4
    Tavronitis
    Hania, Crete
    Greece